



HAL
open science

UUAT1 Is a Golgi-Localized UDP-Uronic Acid Transporter That Modulates the Polysaccharide Composition of Arabidopsis Seed Mucilage

Susana Saez-Aguayo, Carsten Rautengarten, Henry Temple, Dayan Sanhueza,
Troy Ejsmentewicz, Omar Sandoval-Ibañez, Daniela Doñas, Juan Pablo
Parra-Rojas, Berit Ebert, Arnaud Lehner, et al.

► **To cite this version:**

Susana Saez-Aguayo, Carsten Rautengarten, Henry Temple, Dayan Sanhueza, Troy Ejsmentewicz, et al.. UUAT1 Is a Golgi-Localized UDP-Uronic Acid Transporter That Modulates the Polysaccharide Composition of Arabidopsis Seed Mucilage. *The Plant cell*, 2017, 29 (1), pp.129-143. 10.1105/tpc.16.00465 . hal-01775831

HAL Id: hal-01775831

<https://hal.science/hal-01775831>

Submitted on 1 Jun 2018

HAL is a multi-disciplinary open access archive for the deposit and dissemination of scientific research documents, whether they are published or not. The documents may come from teaching and research institutions in France or abroad, or from public or private research centers.

L'archive ouverte pluridisciplinaire **HAL**, est destinée au dépôt et à la diffusion de documents scientifiques de niveau recherche, publiés ou non, émanant des établissements d'enseignement et de recherche français ou étrangers, des laboratoires publics ou privés.

1 RESEARCH ARTICLE

2
3 **UUAT1 Is a Golgi-Localized UDP-Uronic Acid Transporter that Modulates the**
4 **Polysaccharide Composition of Arabidopsis Seed Mucilage.**

5
6 Susana Saez-Aguayo^a, Carsten Rautengarten^b, Henry Temple^a, Dayan Sanhueza^a, Troy
7 Ejsmentewicz^a, Omar Sandoval-Ibañez^a, Daniela Doñas^a, Juan Pablo Parra-Rojas^a, Berit Ebert^b,
8 Arnaud Lehner^c, Jean-Claude Mollet^c, Paul Dupree^d, Henrik V. Scheller^{e,f}, Joshua L. Heazlewood^{b,e},
9 Francisca C. Reyes^{a,1} and Ariel Orellana^{a,1}.

10
11 ^a Centro de Biotecnología Vegetal, FONDAF Center for Genome Regulation, Facultad de Ciencias
12 Biológicas, Universidad Andrés Bello, Santiago, Chile.

13 ^b ARC Centre of Excellence in Plant Cell Walls, School of BioSciences, The University of Melbourne,
14 Victoria 3010, Australia.

15 ^c Normandy University, UniRouen, Laboratoire de Glycobiologie et Matrice Extracellulaire Végétale,
16 EA4358, IRIB, VASI, France.

17 ^d Department of Biochemistry, University of Cambridge, Cambridge CB2 1QW, UK

18 ^e Joint BioEnergy Institute and Biological Systems and Engineering Division, Lawrence Berkeley
19 National Laboratory, Berkeley, CA 94702, USA.

20 ^f Department of Plant and Microbial Biology, University of California, Berkeley, CA 94720, USA.

21
22 Address correspondence to aorellana@unab.cl or francisca.reyes.marquez@gmail.com

23
24 The author responsible for distribution of materials integral to the findings presented in this article in
25 accordance with the policy described in the Instructions for Authors (www.plantcell.org) is: Ariel
26 Orellana (aorellana@unab.cl).

27
28 **Short title:** UUAT1 defines the mucilage sugar content

29
30 **One-sentence summary:** Screening of Arabidopsis mutants with altered seed mucilage allowed
31 identification of UUAT1, a Golgi-localized protein that transports UDP-glucuronic acid and plays a role
32 in the biosynthesis of pectin.

33
34 **Abstract**

35 UDP-glucuronic acid (UDP-GlcA) is the precursor of many plant cell wall polysaccharides, and is
36 required for production of seed mucilage. Following synthesis in the cytosol, it is transported into the
37 lumen of the Golgi apparatus, where it is converted to UDP-galacturonic acid (UDP-GalA), UDP-
38 arabinose and UDP-xylose. To identify the Golgi-localized UDP-GlcA transporter, we screened
39 *Arabidopsis thaliana* mutants in genes coding for putative nucleotide sugar transporters for altered
40 seed mucilage, a structure rich in the GalA-containing polysaccharide rhamnogalacturonan I. As a
41 result, we identified *UUAT1*, which encodes a Golgi-localized protein that transports UDP-GlcA and
42 UDP-GalA in vitro. The seed coat of *uuat1* mutants had less GalA, rhamnose, and xylose in the
43 soluble mucilage, and the distal cell walls had decreased arabinan content. Cell walls of other organs
44 and cells had lower arabinose levels in roots and pollen tubes, but no differences were observed in
45 GalA or xylose contents. Furthermore, the GlcA content of glucuronoxylan in the stem was not
46 affected in the mutant. Interestingly, the degree of homogalacturonan methylation increased in *uuat1*.
47 These results suggest that this UDP-GlcA transporter plays a key role defining the seed mucilage
48 sugar composition, and that its absence produces pleiotropic effects in this component of the plant
49 extracellular matrix.
50

51 INTRODUCTION

52 The plant cell wall is a complex and dynamic structure that is mainly composed of
53 polysaccharides, with cellulose being a key component. The synthesis of noncellulosic
54 polysaccharides (hemicellulose and pectin) occurs in the Golgi apparatus, where a number
55 of glycosyltransferases (GTs) are located (Liepman et al., 2010; Scheible and Pauly, 2004).
56 GTs transfer the sugar residue from an activated nucleotide donor, in the form of a UDP- or
57 GDP-sugar, to a growing polysaccharide chain. Most GTs are type-II membrane-bound
58 proteins with a catalytic domain facing the Golgi lumen (Sterling et al., 2001; Wulff et al.,
59 2000; Scheible and Pauly 2004). However, most nucleotide sugars utilized by GTs are
60 produced in the cytosol (Bar-Peled and O'Neill, 2011; Bonin et al., 1997; Seifert, 2004).
61 Therefore, the Golgi membrane is a physical barrier blocking access to the active GT site.

62 Nucleotide sugar transporters (NSTs) in the Golgi membrane overcome this topological
63 problem and supply the substrates needed in the Golgi lumen for polysaccharide
64 biosynthesis (Orellana et. al., 2016; Reyes and Orellana, 2008; Temple et al., 2016). In
65 *Arabidopsis thaliana*, the genes encoding for NSTs are similar to those encoding for plastidic
66 triose phosphate translocators (TPTs); and together, 44 NSTs and 7 TPTs, form a gene
67 family of 51 members (Knappe et al., 2003; Rautengarten et al., 2014). To date, a number of
68 these NSTs from *A. thaliana* have been functionally characterized, specifically transporters
69 for GDP-mannose (GDP-Man), GDP-fucose (GDP-Fuc), UDP-galactose (UDP-Gal), UDP-
70 glucose (UDP-Glc), UDP-rhamnose (UDP-Rha) and UDP-xylose (UDP-Xyl) (Bakker et al.,
71 2005; Baldwin et al., 2001; Ebert et al., 2015; Handford et al., 2012, 2004; Norambuena et
72 al., 2002, 2005; Rautengarten et al., 2014; Rautengarten et al., 2016; Rollwitz et al., 2006).

73 Hemicellulose and pectins have diverse structures and sugar compositions, and several
74 nucleotide sugars are required for their synthesis. UDP-glucuronic acid (UDP-GlcA), plays a
75 critical role in noncellulosic polysaccharide synthesis, as it is the precursor for several
76 nucleotide sugars involved in hemicellulose and pectin synthesis. These sugars include
77 UDP-galacturonic acid (UDP-GalA), UDP-Xyl, UDP-arabinose (UDP-Ara) and UDP-apiose
78 (UDP-Api) (Reboul et al., 2011). Therefore, UDP-GlcA is a major precursor required for
79 hemicellulose and pectic polysaccharide synthesis. Substrate interconversion is required for
80 polysaccharide biosynthesis and in *Arabidopsis* leaves, polysaccharides containing sugars
81 derived from UDP-GlcA, account for nearly 50% of the cell wall biomass (Zablackis et al.,
82 1995). The cytosol contains some of the enzymes for the interconversion of UDP-GlcA, such
83 as soluble UDP-xylose synthase (UXS) (Harper and Bar-Peled, 2002; Pattathil et al., 2005;
84 Kuang et al., 2016), UDP-apiose/UDP-xylose synthase (Guyett et al., 2009, Mølhøj et al.,
85 2003;) and UDP-arabinose mutase (Konishi et al., 2007; Rautengarten et al., 2011). There
86 are also Golgi-localized interconverting enzymes. These include UDP-glucuronate

87 epimerase (GAE), which converts UDP-GlcA into UDP-GalA (Gu and Bar-Peled, 2004;
88 Mølhøj et al., 2004), membrane attached UXS (Harper and Bar-Peled, 2002; Kuang et al.,
89 2016) and UDP-xylose-4-epimerase, which catalyzes UDP-Xyl to UDP-arabinopyranose
90 (UDP-Arap) epimerization (Burget et al., 2003). All these enzymes are predicted type-II
91 membrane proteins, and their catalytic domain faces the lumen. Therefore, the transport of
92 UDP-GlcA into the Golgi lumen is a critical step for UDP-GalA biosynthesis, as well as for
93 part of the luminal UDP-Xyl. Additionally, UDP-Arap produced from lumen-synthesized UDP-
94 Xyl may rely on this transporter. UDP-GlcA transport is also important for glucuronoxylan
95 biosynthesis because this polymer is synthesized in the Golgi lumen, where GlcA units are
96 added to the xylan backbone. A NST that transports UDP-GlcA has been described in *C.*
97 *elegans* and mutations in the protein responsible for this activity lead to an abnormal
98 development in this organism (Berninsone et al., 2000). A Golgi-localized UDP-GlcA
99 transporter is likely to play a critical role in plant cells by providing the substrate precursors
100 needed for pectin and hemicellulose biosynthesis in the Golgi lumen. In this context, this
101 transporter could play an important role in determining the content of plant cell wall sugars
102 that are derived from UDP-GlcA.

103 To identify a UDP-GlcA transporter and analyze its role in defining cell wall composition, we
104 took advantage of the fact that Arabidopsis seeds produce copious amounts of a pectin-rich
105 substance that is referred to as seed coat mucilage. It is comprised of gel-like molecules that
106 are extruded from mature seeds following water imbibition (Saez-Aguayo et al., 2013;
107 Western et al., 2000; Western, 2012; Young et al., 2008). Early visual examination of the
108 mucilage provided evidence of its pectic nature and showed the presence of two distinct
109 mucilage layers. Both layers contain large amounts of the GalA-containing polysaccharides
110 rhamnogalacturonan I (RG-I) and homogalacturonan (HG). RG-I is mostly unbranched in the
111 external layer, the soluble mucilage (SM), and it is branched, having arabinan and galactan
112 side chains in the internal layer, the adherent mucilage (AM) (Macquet et al., 2007 Western
113 et al., 2000; Willats et al., 2001). The AM also contains methylesterified HG and cellulose
114 microfibrils (Macquet et al., 2007; Saez-Aguayo et al., 2013; Western et al., 2004; Willats et
115 al., 2001). Because mucilage contains high pectin levels, changes in the pathway leading to
116 the synthesis of UDP-GalA will alter RG-I or HG synthesis, affecting the seed mucilage
117 formation and composition. Therefore, the seed coat NST expression analysis was
118 combined with a mucilage release-screening assay of NST mutants to select any novel
119 NSTs potentially involved in the RG-I or HG synthesis. We identified *UUAT1* (*UDP-URONIC*
120 *ACID TRANSPORTER 1*), a gene encoding a protein that can transport UDP-GlcA and
121 UDP-GalA in vitro. A knockout line lacking *UUAT1* has less galacturonic acid (GalA) and
122 rhamnose (Rha) in both AM and SM, and less Xyl in SM. Also, a decrease in arabinan

123 content was observed in the seed coat. Analyses of *UUAT1* expression in other organs and
124 cells revealed differences in Ara content in *uuat1* mutant vs. wild type tissue. Interestingly,
125 besides changes in sugar content, a change in the HG methylation pattern was observed in
126 the mucilage and more methyl groups were released from cell wall material from mucilage
127 and stem, suggesting that HG methylation is also altered in some organs and indicating that
128 pleiotropic changes might take place in the mutant cell wall. Our results suggest that *UUAT1*
129 transports UDP-GlcA in vivo. Furthermore, the loss of function of this transporter leads to
130 changes in monosaccharide composition, in the cell wall, mainly in those sugars related to
131 UDP-GlcA metabolism in the Golgi lumen. These results show the importance of the
132 transport of UDP-GlcA in the biosynthesis of the plant cell wall.

133

134 **RESULTS**

135 **Analysis of NSTs Expressed in Seed Coats and Identification of *UUAT1***

136 In silico data analyses revealed that twenty one out of the fifty one members of the NST/TPT
137 Arabidopsis family (Rautengarten et al., 2014) are expressed in the seed coat during the
138 developmental stages when mucilage is produced and accumulated in epidermal cells
139 (Supplemental Figure 1) (Le et al., 2010; <http://seedgenenetwork.net/arabidopsis>). Of these
140 twenty one candidates, we disregarded those with reported functions (ten known NSTs) in
141 the Arabidopsis UDP-rhamnose/UDP-galactose transporter (URGT) family (Rautengarten et
142 al., 2014), UDP-galactose transporters 1, 2 and 3 UTR1, UTR2, UTR3 (Norambuena et al.,
143 2002, 2005; Reyes et al., 2006, 2010), and GalT1 (Bakker et al., 2005). Among the eleven
144 target genes that were expressed throughout seed development and lack a known function
145 (Supplemental Figure 1), At5g17630 was discarded from the analysis because as it belongs
146 to the triose phosphate translocator clade. Of the ten remaining genes, homozygous mutants
147 could be obtained for seven of them, but only heterozygous mutants were obtained for the
148 other three. Soluble mucilage content was assessed by measuring the uronic acid released
149 following water imbibition. The results showed that a mutant allele of At5g04160, *uuat1*,
150 exhibited the lowest level of mucilage uronic acid (Supplemental Figure 2). *UUAT1*
151 expression was also measured during seed development to confirm that it is expressed
152 during the mucilage production stages (6 to 8 DAP). Supplemental Figure 3 shows a peak in
153 *UUAT1* expression at 8 DAP, a pattern similar to the expression of genes involved in
154 mucilage synthesis (Macquet et al., 2007; Saez-Aguayo et al., 2013; Rautengarten et al.,
155 2014). *UUAT1* encodes a polytopic transmembrane protein with ten putative membrane
156 spanning domains (Supplemental Figure 4) and belongs to a subclade composed of five
157 paralogues with identities ranging from 81% to 49% (Supplemental Table 1). However, their
158 expression levels are much lower than those of *UUAT1* (Supplemental Figure 3).

159 Given these results, we decided to focus on *UUAT1* by analyzing its role in the biosynthesis
160 of seed coat mucilage. Three T-DNA insertion lines were identified in the At5g04160 locus
161 and were designated *uuat1-1*, *uuat1-2* and *uuat1-3* (Figure 1A). These mutant lines had a
162 lower content of GalA and Rha residues in the SM fraction compared to the wild type (WT)
163 Col-0 plants (Figure 1C and Supplemental Table 2). When compared to the other two allelic
164 lines, *uuat1-2* exhibited the most pronounced decrease in both sugars. *UUAT1* transcripts
165 were undetectable in the *uuat1-2* mutant line, whereas the other two lines (*uuat1-1* and
166 *uuat1-3*) exhibited some *UUAT1* expression, albeit at lower levels than WT Col-0 (Figure
167 1B). Thus, we concluded that *uuat1-2* had the strongest phenotype because it was a true
168 knock-out line, whereas the other alleles were knock-down lines and so the studies focused
169 on the *uuat1-2* allele. Molecular rescue of the *uuat1-2* mutant confirmed that the absence of
170 *UUAT1* was responsible for the phenotypes observed in *uuat1-2* (Supplemental Figure 5).
171 The *uuat1-2* line was transformed with a construct that contains the *UUAT1* coding
172 sequence (CDS) fused to a GFP tag and is driven by the *UUAT1* endogenous promoter.
173 Several independent transformants were obtained and the presence of the transgene was
174 confirmed by RT-PCR (Supplemental Figure 5A). Wild-type ruthenium red staining of
175 the AM and sugar content levels were observed in two independent transgenic lines,
176 indicating that *UUAT1*-GFP had successfully rescued the mutant (Supplemental Figure 5B
177 and 5C).

178

179 ***UUAT1* is a UDP-Uronic Acid Transporter in the Golgi**

180 To determine the substrate specificity of *UUAT1* in vitro, it was expressed heterologously in
181 *Saccharomyces cerevisiae* (yeast) and transport assays were conducted as reported in
182 Rautengarten et al (2014). Transport assays were performed using the microsomal proteins
183 reconstituted in proteoliposomes. An immunoblotting analysis of the reconstituted protein
184 confirmed the presence of *UUAT1* in proteoliposomes (Figure 2A). Proteoliposomes were
185 pre-loaded with uridine monophosphate (UMP), guanosine monophosphate (GMP), cytidine
186 monophosphate (CMP) or adenosine monophosphate (AMP) and then incubated with a
187 mixture of 15 nucleotides/nucleotide sugars to determine substrate specificity (Figure 2D,
188 Supplemental Figure 6). Non-transported substrates were removed by gel filtration, and the
189 proteoliposome content analyzed with liquid chromatography-tandem mass spectrometry
190 (LC-MS/MS). The substrate preference exhibited by *UUAT1* could readily be assessed after
191 LC-MS/MS analysis when compared to the empty vector control. *UUAT1* demonstrated clear
192 preferences for UDP-GlcA and UDP-GalA when proteo-liposomes were preloaded with UMP
193 (Figure 2D). No significant differences in transport activity between the control and *UUAT1*

194 were observed for any other nucleotide sugar apart from UDP-Arap, although this activity
195 was much lower than that observed for the UDP-uronic acids (Figure 2D).

196 These substrate preferences were only specific when the proteoliposomes were preloaded
197 with UMP and not with GMP, CMP or AMP (Supplemental Figure 6). Given the additional
198 negative charge present in UDP-uronic acids, UDP was also tested as a potential antiporter
199 substrate, but no transport was observed (Supplemental Figure 6). Proteoliposomes
200 preloaded with GMP could transport GDP-sugars and some lower activity was also observed
201 when proteoliposomes were preloaded with AMP (Supplemental Figure 6), but this is likely
202 to be the result of the endogenous transport activities of the yeast microsomal preparation,
203 since the proteoliposome UUAT1 expression activity did not differ from the control, as has
204 been observed previously (Ebert et al., 2015). UDP-GlcA transport by UUAT1 did not
205 achieve saturation within the concentration range utilized in the assay (Figure 2B), however,
206 transport was affected in a time dependent manner (Figure 2C). Analysis of transport rates
207 indicated that UUAT1 has an apparent K_m of 1.5 mM for UDP-GlcA (Figure 2B).

208 A C-terminal translational fusion with green fluorescent protein (GFP) was used to determine
209 the subcellular localization of UUAT1 using laser scanning confocal microscopy on transient
210 transformed epidermal cells (Figure 3). The UUAT1-GFP distribution pattern was compared
211 with those obtained for the *cis*-Golgi marker α -mannosidase-I (Saint-Jore-Dupas et al.,
212 2006) and an endoplasmic reticulum (ER) marker (Nelson et al., 2007). The fluorescence
213 signal obtained from the UUAT1-GFP protein colocalized with the punctate pattern obtained
214 for the *cis*-Golgi marker α -Man-I but not with the ER marker (Figure 3A to 3F). To confirm
215 the localization of UUAT1, trichomes of transgenic rescued plants expressing UUAT1-GFP
216 under the endogenous promoter were analyzed, and they also showed motile structures
217 exhibiting a punctate pattern, as has been described for Golgi resident proteins (Figure 3G)
218 (Boevink et al., 1998). Taking these data together, these results indicate that UUAT1 is a
219 Golgi-localized UDP-uronic acid transporter.

220

221 **Absence of *UUAT1* Has Pleiotropic Effects on Seed Coat Cell Walls and Mucilage**

222 In order to better understand the effects on the composition of cell wall polysaccharides
223 caused by the absence of *UUAT1*, we analyzed the sugar content of the polysaccharides
224 present in the seed mucilage (Table 1) in both WT Col-0 and *uuat1-2* mutant plants. The
225 SM, as expected, contained mostly GalA and Rha. However, decreases in both GalA (20%)
226 and Rha (22%) were observed in the *uuat1-2* mutant compared to the WT (Table 1).
227 Interestingly, despite the low Xyl levels in the sample, it displayed a similar reduction (21%).
228 Furthermore, the seed+AM fraction from *uuat1-2* showed a 5% decrease in GalA content

229 along with a 9% reduction in Rha (Table 1).

230 To further investigate the differences observed in the Seed+AM fraction and to better
231 understand which polysaccharides might be altered in the mutant, we performed whole
232 mount immunolabeling assays using antibodies against the epitopes present in cell wall
233 polysaccharides, (Figure 4). Based on the measured monosaccharide composition and
234 considering the mucilage polysaccharide composition, the labeling was performed using the
235 following antibodies: CCRC-M36 (anti-RG-I), LM6 (anti-arabinan), JIM7 and LM20 (both anti-
236 methylated HG) (Macquet et al., 2007; Verhertbruggen et al., 2009; Willats et al., 2001). In
237 addition, to visualize the cell wall, we used calcofluor or propidium iodide which stain β -1,4
238 glucans and polysaccharides. RG-I labeling, was reduced in the AM of *uuat1-2* seeds
239 compared to WT Col-0 seeds (Figures 4A and 4C, green signal). Moreover, the calcofluor
240 labeling showed a distal cell wall defect in the mutant when compared with WT Col-0
241 (Figures 4B and 4D, pink labeling), likely due to an abnormal cell wall rupture. The LM6
242 antibody showed less arabinan in the *uuat1-2* AM compared to the WT Col-0, especially in
243 the distal wall of the epidermal cells (Figures 4E and 4F). The lack of staining with the LM6
244 antibody was restored in the transgenic plants that expressed *UUAT1-GFP* with the
245 endogenous promoter (Supplemental Figure 7), providing further evidence that this
246 phenotype is due to the *UUAT1* absence.

247 As the rupture of the distal cell wall upon water imbibition seemed to be altered, we
248 reasoned that the cell wall stiffness might have changed. Because the degree of HG
249 methylation affects the stiffness of the cell wall (Peaucelle et al., 2008), the LM20 and JIM7
250 antibodies were used to look at the highly methylesterified HG distribution (Figure 5 and
251 Supplemental Figure 8). An increase in LM20 labeling in AM was observed in the *uuat1-2*
252 mutant when compared to WT Col-0 (Figures 5 A and 5B), suggesting the presence of HG
253 with a higher degree of methyl esterification in the mutant. This result was also observed
254 using the JIM7 antibody in the allelic lines *uuat1-1* and *uuat1-3* (Supplemental Figure 8).
255 Analysis of the *uuat1-2* lines expressing *UUAT1* supported this observation by showing less
256 labelling than in the mutant, but more labelling than in the WT Col-0 when JIM7 and LM20
257 were used to assess the methylated HG content (Supplemental Figure 7). In addition, we
258 performed ruthenium red staining in the presence of EDTA, a chelator that removes cations
259 and increases the exposure of carboxylic groups, thus enhancing the ruthenium red staining
260 (Figures 5C and 5D). WT Col-0 seeds showed intense staining but mutant seeds exhibited a
261 pale color, suggesting that fewer carboxylic groups were available for binding the dye
262 (Figure 5D). To confirm changes in HG methylesterification in the *uuat1-2* mutant, the
263 contents of methyl groups present in the soluble mucilage and seed+AM fractions were
264 determined by measuring the methanol released upon saponification. Both fractions

265 displayed greater methanol release of 37% and 67%, respectively (Figure 5E). Finally, these
266 HG methylesterification changes correlated with a 10% decrease in pectin methylesterase
267 activity (PME), measured in dry mutant seeds (Figure 5F). All these results provide strong
268 evidence that *UUAT1* absence leads to an increase of highly methylesterified HG epitopes in
269 mucilage.

270

271 **UUAT1 Functions in Different Plant Organs**

272 We next analyzed the *UUAT1* expression pattern in organs such as roots, seedlings, rosette
273 and cauline leaves, stems, flowers, siliques and seeds at different development stages
274 (Supplemental Figure 9). The *UUAT1* transcript was detected by qPCR in all organs
275 analyzed, with expression peaking in stems and flowers (Supplemental Figure 9A). The GUS
276 reporter gene (Jefferson, 1989) was cloned under the control of the *UUAT1* promoter and
277 transformed into WT Col-0 plants to obtain spatial information regarding *UUAT1* expression.
278 Strong GUS activity was detected in roots, seedlings, trichomes, flowers and developing
279 seeds (Supplemental Figure 9B), confirming that *UUAT1* is predominantly expressed in
280 these organs.

281 All obvious phenotypes in the *uuat1-2* mutant were examined first to investigate whether the
282 *UUAT1* mutation leads to changes in plant development and or cell wall composition in
283 organs or tissues apart from the seed mucilage. Interestingly, the only change observed was
284 in the primary stem, as *uuat1-2* plants displayed an early elongation phenotype when
285 compared to WT Col-0 plants (Figure 6A). However, this morphological difference
286 disappeared once the plants reached a mature stage. No changes were observed in sugar
287 composition of the stem cell wall for any of the sugars analyzed, including Xyl (Figure 6C),
288 the most abundant sugar due to the presence of glucuronoxylan, one of the more abundant
289 stem polymers. Because glucuronoxylan also contains GlcA in a given branching frequency,
290 a carbohydrate gel electrophoresis (PACE) polysaccharide analysis (Mortimer et al., 2010)
291 was used to quantify the oligosaccharides Xyl, Xyl₂, and GlcAXyl₄/[MeGlcA] Xyl₄ released by
292 xylanase GH11. No changes were found in the GlcA/Xyl ratio, suggesting that the
293 glucuronoxylan structure is normal in the *uuat1-2* mutant (Figure 6D). Additionally, because
294 changes were observed in mucilage HG methylesterification, this modification was further
295 analyzed in three development stages in stems. The methylesterification levels were
296 observed to be significantly higher in all conditions in the *uuat1-2* mutant when compared to
297 WT Col-0 (Figure 6B).

298 The alcohol insoluble residue (AIR) sugar composition in *uuat1-2* mutant roots, trichome,
299 and pollen tube preparations was analyzed to uncover any possible changes in cell wall

300 composition in other *UUAT1* expressing organs (Figure 7). Ara levels were reduced in roots
301 and pollen tubes. A slight decrease was observed in trichomes but it was not significant. No
302 decrease in GalA or Xyl was observed in any other of the tissues analyzed; thus, Ara was
303 the only sugar whose content consistently decreased in the mutant and this decrease was
304 tissue-specific. In conclusion, our results indicate that plants lacking *UUAT1* show changes
305 in the composition of cell wall monosaccharides derived from the metabolism of UDP-GlcA in
306 the Golgi, with arabinose being the most affected. Furthermore, mutants in *UUAT1* show
307 enhanced levels of methylesterification in cell wall polysaccharides, a likely response to cope
308 with changes in cell wall composition.

309

310 **DISCUSSION**

311 UDP-GlcA is synthesized and utilized in the plant cell cytosol, but it is also required in the
312 Golgi lumen for synthesis of UDP-GalA, UDP-Xyl and UDP-Arap. Therefore, UDP-GlcA
313 needs to be transported from the cytosol across the Golgi membrane into the Golgi lumen to
314 be converted into these nucleotide sugars. Our work led to the identification of *UUAT1*, a
315 protein that can transport UDP-GlcA, UDP-GalA and low levels of UDP-Arap *in vitro*.
316 However, *UUAT1* is unlikely to transport significant amounts of UDP-GalA or UDP-Arap *in vivo*,
317 because both UDP-GlcA 4-epimerase and UDP-Xyl 4-epimerase, the enzymes
318 involved in the synthesis of UDP-GalA and UDP-Arap respectively, are located in the Golgi
319 lumen (Burget et al., 2003; Gu and Bar-Peled, 2004; Mølhøj et al., 2004). A cytosolic
320 salvage pathway for UDP-GalA has been reported (Yang et al., 2009), but requires release
321 from the cell wall of GalA, which can then be converted into UDP-GalA by the enzymes GalA
322 kinase and Sloppy, a promiscuous UDP-sugar pyrophosphorylase (Kotake et al., 2007).
323 Therefore, this salvage pathway may be active only under certain circumstances and
324 perhaps cytosolic UDP-GalA formed via this pathway could be transported by *UUAT1*. UDP-
325 Arap can also be biosynthesized by *UGE1* and *UGE3* in the cytoplasm, using UDP-Xyl to
326 form UDP-Arap. This would presumably be in addition to their roles in the UDP-Glc to UDP-
327 Gal epimerization. However, mutations in these genes suggest that this cytosolic pathway is
328 less important than that located in the Golgi (Rösti et al., 2007; Kotake et al., 2009;
329 Rautengarten et al., 2011; Kotake et al., 2016). Furthermore, because *UUAT1* did not exhibit
330 *in vitro* transport activity for UDP-Araf (arabinose in its furanose form), we postulate that the
331 main *in vivo* role for *UUAT1* is to transport UDP-GlcA to the Golgi lumen. Finally, we believe
332 the low UDP-Arap activity observed is not a function specific to *UUAT1*, because it is also
333 observed in other nucleotide sugar transporters such as the UDP-Rha/UDP-Gal transporters
334 and the UDP-Xyl transporter (Ebert et al., 2015; Rautengarten et al., 2014)

335 *UUAT1* is expressed in seed coat epidermal cells and knockout plants showed a number of
336 mucilage-related phenotypes. The *uuat1-2* mutant displayed reduced GalA and Rha content
337 in both the SM and the seed+AM fraction. Thus, the GalA decrease could be explained by a
338 lower UDP-GlcA transport rate to the Golgi lumen, the substrate required for the UDP-GalA
339 synthesis. Thus, its reduced transport rate could lead to lower levels of this nucleotide sugar
340 in the mutant. On the other hand, *UUAT1* does not transport UDP-Rha, so the Rha decrease
341 is likely due to an impairment in synthesis of the RG-I backbone, which is composed of
342 repeating (GalA-Rha)_n disaccharide units. Because one of the substrates (UDP-GalA) is
343 reduced, it is likely that Rha incorporation has been also affected, leading to lower levels of
344 this sugar in SM and the seed+AM fraction. Something similar occurs in mutants in *URGT2*,
345 a UDP-Rha transporter that is also expressed in seed coat epidermal cells. SM in this
346 mutant also exhibits lowered Rha and GalA, even though *URGT2* does not transport UDP-
347 uronic acids (Rautengarten et al., 2014). The GalA and Rha decrease observed in mucilage
348 (a RG-I enriched matrix) from UDP-Rha and UDP-GlcA transporter mutants suggests a
349 coordination in the supply of both nucleotide sugars during RG-I biosynthesis.

350 The *uuat1* mutants exhibit a decrease in arabinan in AM, as detected by LM6 antibody
351 immunolabeling. Ara is an abundant sugar in the seed+AM fraction and can be present in
352 other polysaccharides (Western et al., 2001), so changes in the total Ara content may not
353 reveal the differences in a low-abundant Ara-containing polymer. The use of antibodies can
354 detect precise changes in arabinan, which is present in the wild type and almost
355 undetectable in the mutant, suggesting that *UUAT1* plays an important role in providing the
356 precursor for arabinan synthesis. The absence of *UUAT1* also results in a reduction in Xyl in
357 SM. However, this phenotype is different from the one observed for *muci21* and *irx14*,
358 xylosyltransferases mutants that show alterations in epidermal cell mucilage adhesion (Hu et
359 al., 2016; Voiniciuc et al., 2015; Ralet et al., 2016). On the other hand, no Xyl changes were
360 observed in the seed+AM fraction, suggesting a precise and discrete role for *UUAT1* in Xyl-
361 containing polymer synthesis.

362 The results show that both the SM and seed+AM matrices in the *uuat1* mutants have lower
363 levels of sugars (GalA, Xyl and Ara) provided by UDP-sugars derived from the metabolism of
364 UDP-GlcA in the Golgi. This supports the role of *UUAT1* as an in vivo UDP-GlcA transporter.
365 Because these sugars are not completely diminished, it suggests that other UDP-GlcA
366 transporters are present in seed coat epidermal cells. Alternatively, some compensatory
367 mechanisms, such as UDP-Xyl transport by specific transporters could be activated (Ebert et
368 al., 2015).

369 In addition to the changes in cell wall composition, our calcofluor staining studies revealed
370 that distal cell walls of seed coat epidermal cells exhibited an abnormal rupture upon

371 imbibition. Whether the changes observed in GalA, Rha, Xyl and arabinan are responsible
372 for this feature remains to be determined. However, an interesting observation was that the
373 *uuat1-2* mutant exhibits an increase in the level of HG methylation, a feature that was
374 partially rescued in plants expressing *UUAT1*. The increase in labeling by the LM20 antibody
375 in mucilage correlated with reduced ruthenium red staining, a dye that binds to the HG
376 carboxyl groups, suggesting their blockage by methyl groups. In addition, more methyl
377 groups were released from mucilage derived from *uuat1-2* mutant seeds and lower PME
378 activity was detected. This methylation increase may be the result of the adaptation that
379 takes place in the *uuat1-2* mutant to compensate for changes in its cell wall. Because the
380 degree of HG methylation correlates to cell wall stiffness, methylation changes may
381 contribute to the altered rupture of distal cell walls during seed imbibition. Regarding HG
382 methylation and arabinan content, it is interesting to note that mutants containing lower HG
383 methylation levels due to defective pectin methyltransferase activity exhibit an increase in
384 Ara (Kim et al., 2015), which could account for higher arabinan levels. By contrast, *uuat1-2*
385 plants show a greater HG methylation and lower arabinan levels, suggesting that an inverse
386 correlation may exist between arabinan content and the degree of HG methylation.

387 The expression pattern of *UUAT1* indicates that it might have additional functional roles in
388 other organs or cell types. Indeed, an evaluation of the cell wall sugar composition of other
389 organs and cells from the *uuat1-2* mutant showed lower levels of Ara in roots and pollen
390 tubes, but not a decrease in Xyl or GalA. These results suggest that changes in the mutant
391 plant cell wall composition are organ-dependent. In this sense, Ara is the sugar most
392 affected in the organs evaluated, suggesting that the supply of UDP-Ara for
393 arabinosyltransferases is more affected in *uuat1-2* plants. On the other hand, the levels of
394 GalA and Xyl did not exhibit significant differences in the mutant, except in seeds. These
395 results could be explained due to redundancy of paralogue genes present in subclade V of
396 the NST gene family (Rautengarten et al., 2014), which could supply UDP-GlcA for the UDP-
397 GalA synthesis. This explanation is also valid for the absence of Xyl changes, but it is
398 important to mention that UDP-Xyl levels in the Golgi lumen are also directly controlled by a
399 UDP-Xyl transporter (UXT1), described recently by Ebert et al. (2015). Mutants in this
400 transporter had decreased Xyl content in stems, and glucuronoxylan was strongly affected
401 (Ebert et al., 2015), suggesting that the UDP-Xyl biosynthesized by cytosolic UXS and
402 transported by UXT1 may be required for xylan synthesis. Furthermore, an *Arabidopsis*
403 cytosolic UXS triple mutant was shown to have an irregular xylem phenotype, while the
404 luminal UXS triple mutant had no Xyl-associated phenotype (Kuang et al., 2016). These
405 findings suggest that *UUAT1* is less important in the synthesis of Xyl-containing
406 polysaccharides. Furthermore, it is likely that the UDP-Xyl made in the cytosol is used to

407 synthesize Xyl-containing polysaccharides, whereas the UDP-Xyl made in the Golgi lumen
408 could be used for the synthesis of UDP-Arap in a tissue-specific manner. However, more
409 data will be required to confirm this hypothesis. No changes were observed in the GlcA/Xyl
410 ratio of glucuronoxylan, one of the main polymers containing GlcA, supporting the idea of
411 redundancy in the UDP-GlcA transport.

412 Cell walls of the *uuat1-2* mutant also exhibited other pleiotropic changes in sugar
413 composition and HG methylation depending on the tissue analyzed. For instance, a Gal
414 decrease was observed in roots, and a GalA increase occurred in pollen tubes. HGs can
415 modulate cell wall stiffness in pollen tubes (Parre and Geitmann, 2005a), and callose content
416 changes may also have an impact on the cell wall mechanics of pollen tubes (Parre and
417 Geitmann 2005b). Consequently, these changes may be a response to the Ara change
418 observed in the *uuat1-2* mutant. Stems also showed methylation increases at different
419 development stages, which correlate with an early plant bolting phenotype. These pleiotropic
420 events may correspond to adaptations of the mutant due to the absence of *UUAT1* and are
421 an indication of the plasticity displayed by the plant cell wall.

422

423 **METHODS**

424 **Plant Material and Growth Conditions**

425 Unless specified otherwise, *Arabidopsis* (*Arabidopsis thaliana* (L.) Heynh) and tobacco
426 (*Nicotiana benthamiana* Domin) plants were germinated and grown in a growth chamber
427 using a long-day regime (16 h photoperiod), the light intensity was $100 \mu\text{mol m}^{-2} \text{s}^{-1}$ and the
428 temperature 21°C. For seeds and aerial tissue collection, plants were grown in soil (Terracult
429 blue substrate, Terracult GmbH) supplemented with fertilizer (Basacote plus 6M, Compo
430 Expert) in a relative humidity (RH) of 60%. The plants were grown in MS media (Duchefa)
431 (2.155 g/L), 1% sucrose and 0.8% agar to obtain root material. T-DNA insertion lines for
432 *UUAT1* (SALK_124146C/ *uuat1-1*, SALK_105023C/ *uuat1-2* and SALK_048507/ *uuat1-3*)
433 were obtained from the Arabidopsis Biological Resource Center (ABRC, <http://abrc.osu.edu/>)
434 using the SIGnAL Salk collection (Alonso et al., 2003). SALK_105023C was annotated as
435 *uuat1-2*. Wild type Columbia-0 (WT Col-0) and mutants were transformed using
436 *Agrobacterium tumefaciens* (GV3101::pMP90) carrying the specified vectors, using the
437 standard floral dip method (Clough and Bent, 1998).

438 **Infiltration of Tobacco Leaves and Subcellular Localization of UUAT1-GFP**

439 Six week-old tobacco leaves were infiltrated with *Agrobacterium tumefaciens*, strain
440 GV3101::pMP90 as described in (Batoko et al., 2000). Two independent transformations
441 were undertaken for analyzing *UUAT1* subcellular localization. ER localization was analyzed

442 using *UUAT1*-GFP and the ER marker AtWAK-mCherry-HDEL (Wall Associated Kinase-2
443 carrying an ER retention signal). Golgi localization was analyzed by cotransformation of
444 *UUAT1*-GFP and the Golgi localized protein α -mannosidase I (α -mannosidase I-mCherry;
445 Nelson et al 2007). Fluorescent signals were analyzed 60 h after infiltration by confocal laser
446 scanning microscopy, using an Olympus FluoView FV1000 spectral microscope.

447 **GUS Staining**

448 The histochemical localization of β -glucuronidase (GUS) activity was performed as
449 described in Jefferson (1989). Tissues were imaged using an Olympus SZ61 stereoscopic
450 microscope and seeds were analyzed with an Olympus Fluoview FV1000 confocal
451 microscope. 488 nm excitation and emission of 485 nm and 491 nm were used for the
452 analysis of seed GUS staining by confocal microscopy, (Truernit et al., 2008).

453 **Ruthenium Red Staining**

454 Mucilage released from mature dry seeds was stained either directly with 0.03% (w/v)
455 ruthenium red or after imbibition in 0.5 M EDTA, pH 8.0, for 90 min. After EDTA treatment,
456 seeds were stained for 2 min and observed with a light microscope (Olympus SZ61).

457 **Genotyping**

458 Genomic DNA was extracted from Arabidopsis 7 d-old cotyledons as described in Edwards
459 et al. (1991). PCR was conducted to amplify the wild type and mutant alleles using the
460 primers described in Supplementary Table 3.

461 **Cloning Procedures**

462 The *UUAT1* coding sequence (CDS) without the stop codon was amplified from cDNA
463 prepared from Arabidopsis leaf RNA, using the primers described in Supplemental Table 3.
464 Resulting PCR products were introduced into the pENTR/D TOPO vector according to
465 standard protocols (Life Technologies) to generate the entry clone pENTR-*UUAT1*. The C-
466 terminal GFP fusion under the control of the cauliflower mosaic virus 35S promoter was
467 generated by introducing the *UUAT1* CDS from the entry clone into the gateway destination
468 vector pK7FWG2.0 (Karimi et al., 2002) using LR clonase (Thermo Fisher Scientific). For the
469 rescue construct, the intergenic region (653 bp) between At5g04170 and At5g04160 was
470 defined as the *UUAT1* promoter (*pUUAT1*) and was amplified from Arabidopsis genomic
471 DNA using the primers described in Supplemental Table 3. Resultant PCR products were
472 introduced into the pENTR 5-TOPO vector (Thermo Fisher Scientific) to generate the
473 pENTR5-*pUUAT1* entry clone. Both, C-terminal GFP and HA fusions were obtained by
474 recombining the entry clones pENTR-*UUAT1* and pENTR5-*pUUAT1* with destination vectors
475 R4pGWB504 and R4pGWB513, respectively. For the transcriptional fusion of *pUUAT1* to the

476 *GUS* reporter gene, the entry clone pENTR5-p*UUAT1* and the destination vector pKGWFS7
477 (Karimi et al., 2002) were recombined using LR clonase (Thermo Fisher Scientific).

478 **Expression Analysis**

479 Total RNA from stems, rosette and cauline leaves, and roots was extracted using Trizol
480 (Thermo Fisher Scientific). For developing seeds, the pollination time in days after pollination
481 (DAP) was defined phenotypically as the time at which the flowers are just starting to open
482 and the long stamens grow over the gynoecium, as previously described in Western et al.,
483 (2000). Seeds were dissected from approximately nine siliques in each DAP for further RNA
484 extraction. RNA extractions were performed using RNeasy Plus Micro Kit, according to
485 manufacturer instructions (Quiagen). 1 µg of total RNA was used as a template for first-
486 strand cDNA synthesis with an oligo (dT) primer and SuperScript II (Thermo Fisher
487 Scientific), according to the manufacturer instructions. The primers described in
488 Supplemental Table 3 were used to amplify PCR products from single-stranded cDNA in the
489 wild type and *uuat1-2* samples for the CDS of *UUAT1* CDS; *EF1αA4*, primers were
490 described in North et al., 2007. Quantitative PCR (qPCR) was performed using the Fast
491 EvaGreen qPCR Master Mix kit (Mx3000P, Stratagene). Reactions contained 1 µL of 1:2
492 diluted cDNA in a total volume of 10 µL. Reactions were carried out using primers that has
493 been previously tested for their efficiency rates and sensitivity in a cDNA dilution series. The
494 quantification and normalization procedures were done using the following equation, as
495 described by Stratagene:

$$496 \quad \text{Normalized} \frac{\text{Unknown}}{\text{Control}} = \frac{(1+E \text{ target})^{-\Delta Ct \text{ target}}}{(1+E \text{ norm})^{-\Delta Ct \text{ norm}}}$$

497 where *E* corresponds to the efficiency of amplification of the target gene, Ct =
498 threshold cycle (Ct), “Control” represents the calibrator sample and norm refers to
499 the reference or normalizer gene. Primers for *UUAT1*, *UUAT2*, *UUAT3*, *UUAT4*, *UUAT5*,
500 *EF1α* (Hong et al., 2010), *UBC9* and seed reference gene At4g12590 (Hong et al., 2010)
501 were those described in Supplemental Table 3.

502 **Analysis of In Vitro *UUAT1* Transport**

503 For heterologous expression, we used the uracil-auxotrophic *Saccharomyces cerevisiae*
504 strain INVSc-1 (*MATa his3D1 leu2 trp1-289 ura3-52 MAT his3D1 leu2 trp1-289 ura3-52*,
505 Thermo Fisher Scientific). The *UUAT1* coding sequence was cloned onto the Gateway
506 expression vector pYES-DEST52 (Thermo Fisher Scientific) and then introduced into the
507 yeast strain with the *S.c.* EasyComp Transformation Kit (Thermo Fisher Scientific). The
508 control was the yeast strain transformed with the empty vector pYES-DEST52. Microsomal
509 fractions were obtained from 200 mL cultures grown at 30°C. Yeast cells were pelleted and

510 spheroplasts produced in 10 mL resuspension buffer (50 mM potassium phosphate, pH 7.1,
511 1.4 M sorbitol, 10 mM NaN₃, and 40 mM 2-mercaptoethanol, 6,000 U Lyticase (Sigma-
512 Aldrich) for 1 h at 37°C. Spheroplasts were harvested by centrifugation and washed with 0.8
513 M sorbitol, 10 mM triethanolamine / acetic acid pH 7.2, 1 mM EDTA. The spheroplasts were
514 lysed with glass beads in 5 mL 0.8 M sorbitol, 10 mM triethanolamine/acetic acid pH 7.2, 1
515 mM EDTA, protease inhibitor cocktail from SIGMA ALDRICH and 1 mM PMSF. Microsomes
516 were isolated by sequential centrifugation (8,000 g for 10 min (F1), and 100,000 g for 75 min
517 (F2)). The F2 fraction was reconstituted in 10 mM Tricine-KOH pH 7.5, 50 mM potassium
518 gluconate, 20% glycerol. Proteoliposomes were generated with acetone-washed soybean L-
519 α -phosphatidylcholine (Avanti Polar Lipids) in reconstitution buffer (10 mM Tricine-KOH pH
520 7.5, 50 mM potassium gluconate and 20% glycerol). Reconstitution of microsomal
521 membranes obtained from the UUAT1-expressing yeast or the control cells was undertaken
522 using approximately 400 μ g microsomal protein in reconstitution buffer, lipid at a ratio of 13:1
523 (lipid:protein), 10 mM exchange substrate and 50 mM octyl- β -glucoside. Unincorporated
524 components were removed from reconstituted liposomes using Sephadex G50 columns (GE
525 Healthcare). 200 μ L Aliquots were incubated with nucleotide sugar substrates at 25°C for the
526 indicated times to assess transporter activities. Kinetic parameters were calculated with non-
527 linear regression using the Prism 7 application (GraphPad Software, La Jolla, CA).
528 Polyacrylamide gel electrophoresis was carried out with 2.5 μ g protein of proteoliposomes
529 on a 7-15% SDS-PAGE gel. Immunoblotting was conducted with the anti-V5 antibody, using
530 a 1:10,000 dilution (Thermo Fisher Scientific).

531 **Nucleotide Sugar Quantification Using Tandem Mass Spectrometry**

532 The transport assay reactions were purified using ENVI-Carb SPE columns (Sigma-Aldrich)
533 and then lyophilized overnight, as outlined in Ito et al., (2014), and then analyzed by tandem
534 mass spectrometry (LC-MS/MS). Nucleotide sugars were separated using a Hypercarb
535 column (150 mm \times 1 mm, 5 μ m) at a flow rate of 50 μ L min⁻¹ with an 1100 series HPLC
536 system (Agilent Technologies, CA) and a 4000 QTRAP LC-MS/MS system (Sciex, CA)
537 equipped with a TurbolonSpray ion source. Initial conditions were 95% buffer A (LC-MS
538 grade water with 0.3% formic acid, pH 9.0 with ammonia) and 5% buffer B (100 %
539 acetonitrile) for 1 min followed by a gradient to 75% (A) in 20 min, then 50% (A) in 5 min
540 before returning to 95% (A) in 5 min. The instrument was operated in negative ion mode,
541 using the multiple reaction monitoring (MRM) scan type. A declustering potential (DP) of -40,
542 entrance potential (EP) of -10, collision cell exit potential (CXP) was -15. The ion spray
543 voltage was set at -4200 V, source temperature (TEM) at 425 °C, collision gas (CAD) was
544 set to High and source gas 1 (GS1) and 2 (GS2) were both set to 20. A time of 100 ms was
545 applied for each transition, resulting in a duty cycle of 1.0501 s with both Q1 and Q3

546 resolution set to Unit. All data were acquired using Analyst 1.6 Build 3773 (Sciex, CA).
547 Nucleotide sugars were quantified using MultiQuant 2.1 (build 2.1.1296.02.1) software
548 (Sciex, CA) by integrating the signal peak areas of samples against a range of nucleotide
549 sugar standards (2.5 to 20 pmol).

550 **Seed Immunolabeling**

551 Immunolabeling was performed with four monoclonal antibodies, CCRC-M36 (labels
552 rhamnogalacturonan-I), LM6 (arabinan), JIM7 (partially methyl-esterified homogalacturonan)
553 and LM20 (highly methyl-esterified homogalacturonan) (Saez-Aguayo et al., 2013). A
554 double labeling with an antibody plus calcofluor white (0.01%) or propidium iodide (20 μg
555 mL^{-1}) was performed as indicated for each antibody to observe the seed surface and AM
556 layer. Optical sections were obtained using an Olympus LX81 spectral confocal laser-
557 scanning microscope. A 488 nm argon laser line was used to excite Alexa Fluor 488, a 405
558 nm diode laser line was used to excite calcofluor white and a 543 nm neon laser line was
559 used to excite propidium iodide. Fluorescence emission was detected between 504 and 579
560 nm for Alexa Fluor 488, 412 and 490 nm for calcofluor white, and 550 nm and 725 nm for
561 propidium iodide. For comparisons of the signal intensity within one experiment, the laser
562 gain values were fixed.

563 **Trichome Isolation**

564 Trichome isolation was performed as described in Marks et al. (2008), with slight
565 modifications. The aerial parts of 18 d-old seedlings were placed in a 50 mL tube with 15 mL
566 of preheated (37°C) phosphate-buffered saline (137 mM KCl, 10 mM K_2HPO_4 , 2 mM
567 KH_2PO_4) containing 100 mM EGTA-KOH (pH 7.5) and 50 mg of glass beads 425-600 μm
568 (Sigma-Aldrich). The plant material was then subjected to four cycles at maximum vortex
569 speed for 30 s and on ice for 30 s. The trichomes were recovered using a nylon cell strainer
570 (pore size: 70 μm , BD Falcon) and re-suspended in PBS buffer without EGTA.

571 **Alcohol-Insoluble Residue (AIR) Preparation**

572 Plant tissues were ground in liquid nitrogen and extracted twice in 80% ethanol with agitation
573 for 1 h at room temperature followed by removal of lipids by washing twice with
574 methanol:chloroform (1:1) and twice with acetone. The final alcohol insoluble residue (AIR)
575 was dried overnight at room temperature. A sequential extraction procedure was used for
576 determining the sugar composition of SM and seed+AM,. 20 mg of seeds were imbibed 3
577 times with 1 mL of water for 20 min; the SM was separated by 10 min of centrifugation at
578 12,000 g, lyophilized and resuspended in 300 μL of water before hydrolysis. The AM + seed
579 fraction was lyophilized and AIR preparation was prepared as described above.

580 **Acid Hydrolysis**

581 Two mg AIR were hydrolyzed for 20 min for soluble mucilage and 1h for other tissues with
582 450 μL 2 M trifluoroacetic acid (TFA) at 121 °C. TFA was evaporated at 60°C with nitrogen
583 and the samples were washed twice in 250 μL of 100% isopropanol and dried in a speed-
584 vac. The suspension was clarified by passing through a syringe filter (pore size: 0.45 μm),
585 transferred to a new tube and used for HPAEC-PAD analysis as described below. Inositol
586 was used as the internal control for TFA hydrolysis.

587 **In Vitro Pollen Tube Growth and Cell Wall Extraction**

588 Pollen was grown in vitro in a liquid medium according to the method described in Boavida
589 and McCormick, (2007), Dardelle et al. (2010). Forty freshly opened flowers were
590 submerged in 1 mL of germination medium containing 5 mM CaCl_2 , 0.01% (w/v) H_3BO_3 , 5
591 mM KCl, 1 mM MgSO_4 , and 10% (w/v) sucrose (pH 7.5), and tubes were shaken with a
592 vortex to release the pollen grains from the anthers. Flowers were removed with a pair of
593 tweezers, and the pollen suspension was then pelleted at 3,200 g for 6 min. New GM (250
594 μL) was added to the pellet, and pollen grains were grown in a growth chamber in the dark
595 at 22°C for 6 h. Before any further manipulation, pollen germination and pollen tube growth
596 were assessed with an inverted microscope. After 6 h, three volumes of 95% ethanol were
597 added to the GM and stored at 4°C until use. Six h-old pollen tubes from 480 flowers were
598 pooled, centrifuged at 5,000 g and rinsed three times with 1 mL of 70% ethanol to remove
599 salts and sucrose. The insoluble material was ground and treated three times with 70%
600 ethanol at 70°C for 15 min followed by an incubation with 1 mL of a mixture of
601 chloroform:methanol (1:1, v/v) for 15 min. After centrifugation (12,000 g for 10 min), the
602 remaining insoluble material was dried to yield the AIR fraction (about 1 mg). This
603 experiment was performed three times.

604 **Methylesterification Analysis of AIR Samples**

605 The degree of methylesterification of WT Col-0 and *uuat1-2* was analyzed in 2 mg of AIR
606 preparations from roots or seeds with AM. For SM, 5 mg of seeds were imbibed in 200 μL of
607 ultrapure water for 6 h, as described in Anthon and Barrett, (2004). All experiments were
608 done using 3 technical replicates and at least 2 biological replicates.

609 **High Performance Anion Exchange Chromatography with Pulsed Amperometric** 610 **Detection (HPAEC-PAD)**

611 A Dionex ICS3000 ion chromatography system, equipped with a pulsed amperometric
612 detector, a CarboPac PA1 (4 mm x 250 mm) analytical column and a CarboPac PA1 (4 mm
613 x 50 mm) guard column was used to quantify sugars. The separation of neutral sugars was

614 performed at 40°C with a flow rate of 1 mL/min using an isocratic gradient of 20 mM NaOH
615 for 20 min followed by a wash with 200 mM NaOH for 10 min. After every run, the column
616 was equilibrated in 20 mM NaOH for 10 min. Separation of acidic sugars was performed
617 using 150 mM NaOAc and 100 mM NaOH for 10 min at a flow rate of 1 mL/min at 40°C.
618 Standard curves of neutral sugars (D-Fuc, L-Rha, L-Ara, D-Gal, D-Glc, D-Xyl, and D-Man) or
619 acidic sugars (D-GalA and D-GlcA) were used for quantification.

620 **Determination of Monosaccharide Composition of Pollen Tubes Using Gas** 621 **Chromatography–Flame Ionization Detection (GC-FID)**

622 Samples were prepared as described in Dardelle et al., 2014. Approximately 0.5 mg of
623 sample was hydrolyzed with 2 M TFA for 2 h at 110°C. Monosaccharides were then
624 derivatized with 1 M methanol-HCl at 80°C overnight followed by a mixture of
625 hexamethyldisiloxan:trimethyldisiloxan:pyridine (3:1:9) at 110°C for 20 min. After drying,
626 derivatives were dissolved in 1 mL of cyclohexane and injected into the 3800 GC system
627 equipped with a CP-Sil5-CB column. A temperature gradient from 120 to 160°C at 10°C min⁻¹,
628 160 to 220°C at 1.5°C min⁻¹ and 220 to 280°C at 20°C min⁻¹ was used. Quantification was
629 based on the internal standard and response factors previously determined for each
630 monosaccharide.

631 **Determination of PME Activity**

632 Total protein extraction and PME activity assays were performed as described in Saez-
633 Aguayo et al. (2013). Measurements of stained areas to determine PME activity were
634 obtained using the ImageJ software (Abramoff et al., 2004)

635 **Analysis of Stem Xylan Using PACE**

636 AIR preparations and PACE were performed as described by Mortimer et al. (2010). One mg
637 of AIR from basal stems were incubated overnight in 0.1 M ammonium acetate buffer
638 (pH5.5) with an excess of *Neocallimastix patriciarum* Xyn11A xylanase at 21°C.
639 Samples were derivatized with 8-aminonaphthalene-1,3,6-trisulphonic acid (ANTS;
640 Invitrogen). After drying in vacuo, the samples were resuspended in 3 M urea (100
641 µL), of which 5 µL was loaded onto the PACE gels. Samples were electrophoresed
642 for 30 min at 200 V and then for 100 min at 1,000 V. Gels were visualized using a
643 Genebox (Syngene) equipped with a transilluminator with long-wave tubes emitting
644 at 365 nm and a short-pass (500–600 nm) filter. The quantity of each of the
645 oligosaccharides released by Xyn11A [Xyl, (Xyl)₂, GlcA-(Xyl)₄/ Me-GlcA(Xyl)₄] as well
646 as the GlcA/Xyl ratio could be calculated by using the analytical software Genetools

647 (Syngene). Results presented correspond to 4 biological replicates. The enzyme was
648 a kind gift of Harry Gilbert (University of Newcastle, UK).

649 **Accession Numbers**

650 Nucleotide sequences for Arabidopsis *UUAT1* have been deposited in GenBank (Benson et
651 al., 2012) under accession numbers KT923621 (At5g04160, coding sequence) and
652 KT923622 (At5g04160, promoter). T-DNA insertion lines in the At5g04160 locus were
653 obtained from the Arabidopsis Biological Resource Center: *uuat1-1* (SALK_124146C),
654 *uuat1-2*, (SALK_105023C) and *uuat1-3* (SALK_048507).

655 **Supplemental Data**

656 **Supplemental Figure 1.** NST Genes Expressed During Seed Development..

657 **Supplemental Figure 2.** Uronic Acid Content in the Soluble Mucilage Fraction from
658 Mutants in NST Genes.

659 **Supplemental Figure 3.** *UUATs* Expression in Developing Seeds.

660 **Supplemental Figure 4.** *UUAT1* Hydropathy Plot

661
662 **Supplemental Figure 5.** Rescue of the *uuat1-2* Mutant Phenotype Using the
663 *UUAT1 ProUUAT1:UUAT1-GFP* Construct.

664 **Supplemental Figure 6.** Exchange of Nucleotide Sugars with GMP, AMP, CMP or UDP by
665 *UUAT1*.

666 **Supplemental Figure 7.** Analyses of the Mucilage Phenotypes of *uuat1-2* and the Rescued
667 Lines Using Immunolocalization.

668 **Supplemental Figure 8.** Changes in Methylesterification Degree in *uuat1* Allelic Mutants.

669 **Supplemental Figure 9.** *UUAT1* is Highly Expressed in Roots, Trichomes, Stems and Seed
670 Coat.

671 **Supplemental Table 1.** Percentage of Protein Identity among *UUATs* Family Members.

672 **Supplemental Table 2.** Sugar Composition of Soluble Mucilage from WT Col-0 and *uuat1*
673 Allelic Lines.

674 **Supplemental Table 3.** Sequences of Primers Used in this Study.

675

676 **AUTHOR CONTRIBUTIONS**

677 S.S.A, F.C.R, H.V.S., J.L.H. and A.O. designed the research; S.S.A., C.R., B.E., D.S., T.E.,
678 H.T., O.S., D.D., J-P P, A.L, J-C.M., F.C.R. performed the experiments; S.S.A., C.R., H.T., J-
679 C.M., P.D., J.L.H., H.V.S., F.C.R and A.O. analyzed the data; and S.S.A., F.C.R., A.O and
680 H.T. wrote the paper.

681

682 **ACKNOWLEDGEMENTS**

683 This work was supported by FONDECYT 11130498 (to F.C.R), FONDECYT 3140415 (to
684 S.S.A), FONDECYT 1151335, Fondo de Areas Prioritarias-Centro de Regulacion del
685 Genoma-15090007, ECOS-CONICYT C14B02 and PFB-16 (to A.O) and a CONICYT
686 fellowship to H.T. Work conducted by the Joint BioEnergy Institute was supported by the
687 U.S. Department of Energy, Office of Science, Office of Biological and Environmental
688 Research, through contract DE-AC02-05CH11231 between Lawrence Berkeley National
689 Laboratory and the U. S. Department of Energy. J.L.H. is supported by an Australian
690 Research Council Future Fellowship [FT130101165]. Work conducted by Glyco-MEV (J-
691 C.M. and A.L.) was in part supported by the VASI research network from the Upper
692 Normandy region and the French ministry of research. We would like to thank Miriam Barros
693 for her advice and expertise in confocal microscopy. We are also grateful to Hernan Salinas
694 and Alvaro Miquel for technical assistance with HPAEC analysis, to Flavien Dardelle and
695 François Le Mauff for technical assistance with GC analyses of pollen tube cell walls.

696

697 **Table 1.** Sugar Composition of Seeds Plus Adherent Mucilage (seed + AM) and Extracted
 698 Soluble Mucilage (SM) from WT Col-0 and *uuat1-2* Plants.

Structure	Sugar	WT Col-0	<i>uuat1-2</i>
<u>Seed +AM</u>	GalA	20.67 (0.21)*	19.68 (0.42)*
	Rha	21.77 (0.77)*	20.02 (0.45)*
	Fuc	1.74 (0.05)	1.72 (0.03)
	Ara	41.21 (1.59)	39.62 (1.06)
	Xyl	11.37 (0.56)	11.45 (0.47)
	Man	3.44 (0.12)	3.69 (0.16)
	Gal	30.23 (0.40)	29.06 (1.13)
	Glc	7.43 (0.26)	8.18 (0.29)
	GlcA	2.44 (0.08)	2.55 (0.07)
Total Seed + AM		140.30 (2.80)	135.96 (1.92)
<u>SM</u>	GalA	5.66 (0.21)*	4,56 (0.22)*
	Rha	8,65 (0.49)*	6.76 (0.43) *
	Ara	0.08 (0.02)	0.09 (0.01)
	Xyl	0.43 (0.02)*	0.34 (0.02)*
	Gal	0.31 (0.04)	0.26 (0.02)
Total SM		15.15 (0.64)	11.99 (0.95)

699

700 To analyze monosaccharide composition, a water-soluble extraction was used to isolate the
 701 SM fraction. The adherent mucilage cannot be detached from the seed and form the seed+
 702 soluble mucilage fraction (seed + MA). Sugar content was obtained using HPAEC-PAD from
 703 seed + AM and from SM. Values are in mg/g of dry seeds and are the means of 3 biological
 704 replicates. Standard errors are shown in parentheses for 2 technical replicates each. (*)
 705 Significant statistical differences using the Wilcoxon test ($p < 0.05$).

706

707

708

709

710 REFERENCES

711

712 **Abramoff, M.D., Magalhães, P.J., and Ram, S.J.** (2004). Image processing with ImageJ.
713 *Biophotonics Int.* **11**: 36–42.

714 **Alonso, J.M., Stepanova, A.N., Leisse, T.J., Kim, C.J., Chen, H., Shinn, P., Stevenson,**
715 **D.K., Zimmerman, J., Barajas, P., Cheuk, R., et al.** (2003). Genome-wide insertional
716 mutagenesis of *Arabidopsis thaliana*. *Science* **301**: 653–657.

717 **Anthon, G.E., and Barrett, D.M.** (2004). Comparison of three colorimetric reagents in the
718 determination of methanol with Alcohol Oxidase. Application to the assay of Pectin
719 Methyltransferase. *J. Agric. Food Chem.* **52**: 3749–3753.

720 **Bakker, H., Routier, F., Oelmann, S., Jordi, W., Lommen, A., Gerardy-Schahn, R., and**
721 **Bosch, D.** (2005). Molecular cloning of two Arabidopsis UDP-galactose transporters by
722 complementation of a deficient Chinese hamster ovary cell line. *Glycobiology* **15**: 193–201.

723 **Baldwin, T.C., Handford, M.G., Yuseff, M.I., Orellana, A., and Dupree, P.** (2001).
724 Identification and characterization of GONST1, a Golgi-localized GDP-mannose transporter
725 in Arabidopsis. *Plant Cell* **13**: 2283–2295.

726 **Bar-Peled, M., and O'Neill, M.A.** (2011). Plant nucleotide sugar formation, interconversion,
727 and salvage by sugar recycling. *Annu. Rev. Plant Biol.* **62**: 127–155.

728 **Batoko, H., Zheng, H.-Q., Hawes, C., and Moore, I.** (2000). A Rab1 GTPase is required for
729 transport between the endoplasmic reticulum and Golgi apparatus and for normal Golgi
730 movement in plants. *Plant Cell* **12**: 2201–2217.

731 **Benson, D.A., Karsch-Mizrachi, I., Clark, K., Lipman, D.J., Ostell, J., and Sayers, E.W.**
732 (2012). GenBank. *Nucleic Acids Res.* **40**: D48–D53.

733 **Berninsone, P. M., and Hirschberg, C. B.** (2000). Nucleotide sugar transporters of the
734 Golgi apparatus. *Current Opin. Struct. Biol.*, **10**: 542-547.

735 **Boavida, L.C., and McCormick, S.** (2007). Temperature as a determinant factor for
736 increased and reproducible in vitro pollen germination in *Arabidopsis thaliana*. *Plant J.* **52**:
737 570–582.

738 **Boevink, P., Oparka, K., Santa Cruz, S., Martin, B., Betteridge, A., and Hawes, C.**
739 (1998). Stacks on tracks: the plant Golgi apparatus traffics on an actin/ER network. *Plant J.*
740 **15**: 441–447.

741 **Bonin, C.P., Potter, I., Vanzin, G.F., and Reiter, W.-D.** (1997). The MUR1 gene of
742 Arabidopsis thaliana encodes an isoform of GDP-D-mannose-4,6-dehydratase, catalyzing
743 the first step in the de novo synthesis of GDP-L-fucose. *Proc. Natl. Acad. Sci. USA* **94**:
744 2085–2090.

745 **Burget, E.G., Verma, R., Mølhøj, M., and Reiter, W.-D.** (2003). The biosynthesis of L-
746 arabinose in plants: molecular cloning and characterization of a Golgi-localized UDP-D-
747 xylose 4-epimerase encoded by the MUR4 gene of Arabidopsis. *Plant Cell* **15**: 523–531.

748 **Clough, S.J., and Bent, A.F.** (1998). Floral dip: a simplified method for Agrobacterium-
749 mediated transformation of *Arabidopsis thaliana*. *Plant J.* **16**: 735–743.

750 **Dardelle, F., Lehner, A., Ramdani, Y., Bardor, M., Lerouge, P., Driouich, A., and Mollet,**
751 **J.-C.** (2010). Biochemical and immunocytological characterizations of Arabidopsis pollen
752 tube cell wall. *Plant Physiol.* **153**: 1563–1576.

753 **Dardelle, F., Mauff, F.L., Lehner, A., Loutelier-Bourhis, C., Bardor, M., Rihouey, C.,**
754 **Causse, M., Lerouge, P., Driouich, A., and Mollet, J.-C.** (2014). Pollen tube cell walls of

755 wild and domesticated tomatoes contain arabinosylated and fucosylated xyloglucan. *Ann.*
756 *Bot.* **115**: 55-66.

757 **Ebert, B., Rautengarten, C., Guo, X., Xiong, G., Stonebloom, S., Smith-Moritz, A.M.,**
758 **Herter, T., Chan, L.J.G., Adams, P.D., Petzold, C.J., et al.** (2015). Identification and
759 characterization of a Golgi-localized UDP-Xylose transporter family from *Arabidopsis*. *Plant*
760 *Cell* **27**. 1218-1227.

761 **Edwards, K., Johnstone, C., and Thompson, C.** (1991). A simple and rapid method for the
762 preparation of plant genomic DNA for PCR analysis. *Nucleic Acids Res.* **19**. 1349.

763 **Gu, X., and Bar-Peled, M.** (2004). The biosynthesis of UDP-Galacturonic Acid in plants.
764 Functional cloning and characterization of *Arabidopsis* UDP-D-Glucuronic acid 4-epimerase.
765 *Plant Physiol.* **136**. 4256–4264.

766 **Guyett, P., Glushka, J., Gu, X., and Bar-Peled, M.** (2009). Real-time NMR monitoring of
767 intermediates and labile products of the bifunctional enzyme UDP-apiose/UDP- xylose
768 synthase. *Carbohydr. Res.* **344**: 1072–1078.

769 **Handford, M., Rodríguez-Furlán, C., Marchant, L., Segura, M., Gómez, D., Alvarez-**
770 **Buylla, E., Xiong, G.-Y., Pauly, M., and Orellana, A.** (2012). *Arabidopsis thaliana* AtUTr7
771 encodes a golgi-localized UDP-glucose/UDP-galactose transporter that affects lateral root
772 emergence. *Mol. Plant* **5**: 1263–1280.

773 **Handford, M.G., Sicilia, F., Brandizzi, F., Chung, J.H., and Dupree, P.** (2004).
774 *Arabidopsis thaliana* expresses multiple Golgi-localised nucleotide-sugar transporters related
775 to GONST1. *Mol. Genet. Genomics* **272**: 397–410.

776 **Harper, A.D., and Bar-Peled, M.** (2002). Biosynthesis of UDP-xylose. Cloning and
777 characterization of a novel *Arabidopsis* gene family, UXS, encoding soluble and putative
778 membrane-bound UDP-glucuronic acid decarboxylase isoforms. *Plant Physiol.* **130**: 2188–
779 2198.

780 **Hong, S.M., Bahn, S.C., Lyu, A., Jung, H.S., and Ahn, J.H.** (2010). Identification and
781 testing of superior reference genes for a starting pool of transcript normalization in
782 *Arabidopsis*. *Plant Cell Physiol.* **51**: 1694–1706.

783 **Hu, R., Li, J., Wang, X., Zhao, X., Wang, Z., Yang, X., Tang, Q., He, G., Zhou, G., and**
784 **Kong, Y.** (2016). Xylan synthesized by Irregular Xylem 14 (IRX14) maintains the structure of
785 seed coat mucilage in *Arabidopsis*. *J. Exp. Bot.* **67**: 1243-1257..

786 **Ito, N., Ito, K., Ikebuchi, Y., Kito, T., Miyata, H., Toyoda, Y., Takada, T., Hisaka, A.,**
787 **Honma, M., Oka, A. and Kusuhara, H.** (2014). Organic cation transporter/solute carrier
788 family 22a is involved in drug transfer into milk in mice. *J. Pharma. Sci.*, **103**: 3342-3348.

789 **Jefferson R.A.** (1989) The GUS reporter gene system. *Nature*, **342**: 837-838.

790 **Karimi, M., Inzé, D., and Depicker, A.** (2002). GATEWAY vectors for *Agrobacterium*-
791 mediated plant transformation. *Trends Plant Sci.* **7**: 193–195.

792 **Kim, S.-J., Held, M.A., Zemelis, S., Wilkerson, C., and Brandizzi, F.** (2015). CGR2 and
793 CGR3 have critical overlapping roles in pectin methylesterification and plant growth in
794 *Arabidopsis thaliana*. *Plant J.* **82**: 208–220.

795 **Knappe, S., Flügge, U.-I., and Fischer, K.** (2003). Analysis of the plastidic phosphate
796 translocator gene family in *Arabidopsis* and identification of new phosphate translocator-
797 homologous transporters, classified by their putative substrate-binding site. *Plant Physiol.*
798 **131**: 1178–1190.

799 **Konishi, T., Takeda, T., Miyazaki, Y., Ohnishi-Kameyama, M., Hayashi, T., O'Neill, M. A.,**
800 **and Ishii, T.** (2007). A plant mutase that interconverts UDP-arabinofuranose and UDP-
801 arabinopyranose. *Glycobiology*, **17**: 345-354.

802 **Kotake, T., Hojo, S., Yamaguchi, D., Aohara, T., Konishi, T., & Tsumuraya, Y.** (2007).
803 Properties and physiological functions of UDP-sugar pyrophosphorylase in *Arabidopsis*.
804 *Biosci., Biotechnol. Biochem.*, **71**: 761-771.

805 **Kotake, T., Takata, R., Verma, R., Takaba, M., Yamaguchi, D., Orita, T., et al.** (2009).
806 Bifunctional cytosolic UDP-glucose 4-epimerases catalyze the interconversion between
807 UDP-D-xylose and UDP-L-arabinose in plants. *Biochem. J.*, **424**: 169-177

808 **Kotake, T., Yamanashi, Y., Imaizumi, C. and Tsumuraya, Y.** (2016). Metabolism of L-
809 arabinose in plants. *J. Plant Research*, **129**: 781-792.

810 **Kuang, B., Zhao, X., Zhou, C., Zeng, W., Ren, J., Ebert, B., Beahan, C.T., Deng, X.,**
811 **Zeng, Q., Zhou, G., Doblin, M.S., Heazlewood, J.L., Bacic, A., Chen, X., and Wu, A.M.**
812 (2016). The role of UDP-glucuronic acid decarboxylase(s) (UXS) in xylan biosynthesis in
813 *Arabidopsis*. *Mol. Plant* **9**: 1119-1131.

814 **Le, B.H., Cheng, C., Bui, A.Q., Wagmaister, J.A., Henry, K.F., Pelletier, J., Kwong, L.,**
815 **Belmonte, M., Kirkbride, R., Horvath, S., et al.** (2010). Global analysis of gene activity
816 during *Arabidopsis* seed development and identification of seed-specific transcription factors.
817 *Proc. Natl. Acad. Sci. USA* **107**: 8063–8070.

818 **Liepman, A.H., Wightman, R., Geshi, N., Turner, S.R., and Scheller, H.V.** (2010).
819 *Arabidopsis* - a powerful model system for plant cell wall research. *Plant J.* **61**: 1107–1121.

820 **Macquet, A., Ralet, M.-C., Kronenberger, J., Marion-Poll, A., and North, H.M.** (2007). In
821 situ, chemical and macromolecular study of the composition of *Arabidopsis thaliana* seed
822 coat mucilage. *Plant Cell Physiol.* **48**: 984–999.

823 **Marks, M.D., Betancur, L., Gilding, E., Chen, F., Bauer, S., Wenger, J.P., Dixon, R.A.,**
824 **and Haigler, C.H.** (2008). A new method for isolating large quantities of *Arabidopsis*
825 trichomes for transcriptome, cell wall and other types of analyses. *Plant J.* **56**: 483–492.

826 **Mølhøj, M., Verma, R., & Reiter, W. D.** (2003). The biosynthesis of the branched chain
827 sugar D-apiose in plants: functional cloning and characterization of a UDP-D-apiose/UDP-D-
828 xylose synthase from *Arabidopsis*. *Plant J.* **35**: 693-703.

829 **Mølhøj, M., Verma, R., and Reiter, W.-D.** (2004). The biosynthesis of D-Galacturonate in
830 plants. functional cloning and characterization of a membrane-anchored UDP-D-Glucuronate
831 4-epimerase from *Arabidopsis*. *Plant Physiol.* **135**: 1221–1230.

832 **Mortimer, J.C., Miles, G.P., Brown, D.M., Zhang, Z., Segura, M.P., Weimar, T., Yu, X.,**
833 **Seffen, K.A., Stephens, E., Turner, S.R., et al.** (2010). Absence of branches from xylan in
834 *Arabidopsis gux* mutants reveals potential for simplification of lignocellulosic biomass. *Proc.*
835 *Natl. Acad. Sci. USA* **107**: 17409–17414.

836 **Nelson, B.K., Cai, X., and Nebenführ, A.** (2007). A multicolored set of in vivo organelle
837 markers for co-localization studies in *Arabidopsis* and other plants. *Plant J.* **51**: 1126–1136.

838 **Norambuena, L., Marchant, L., Berninsone, P., Hirschberg, C.B., Silva, H., and**
839 **Orellana, A.** (2002). Transport of UDP-galactose in plants. Identification and functional
840 characterization of AtUTr1, an *Arabidopsis thaliana* UDP-galactos/UDP-glucose transporter.
841 *J. Biol. Chem.* **277**: 32923–32929.

842 **Norambuena, L., Nilo, R., Handford, M., Reyes, F., Marchant, L., Meisel, L., and**
843 **Orellana, A.** (2005). AtUTr2 is an *Arabidopsis thaliana* nucleotide sugar transporter located
844 in the Golgi apparatus capable of transporting UDP-galactose. *Planta* **222**: 521–529.

845 **North, H.M., De Almeida, A., Boutin, J.-P., Frey, A., To, A., Botran, L., Sotta, B., and**
846 **Marion-Poll, A.** (2007). The *Arabidopsis* ABA-deficient mutant *aba4* demonstrates that the

847 major route for stress-induced ABA accumulation is via neoxanthin isomers. *Plant J. Cell*
848 *Mol. Biol.* **50**: 810–824.

849 **Orellana, A., Moraga, C., Araya, M., and Moreno, A. (2016).** Overview of Nucleotide
850 Sugar Transporter Gene Family Functions Across Multiple Species. *J. Mol. Biol.* **428**: 3150-
851 3165.

852 **Parre, E, and Geitmann, A. (2005a).** Pectin and the role of the physical properties of the
853 cell wall in pollen tube growth of *Solanum chacoense*. *Planta* **220**: 582-592

854 **Parre, E, and Geitmann, A. (2005b).** More than a leak sealant. The mechanical properties
855 of callose in pollen tubes. *Plant Physiol.* **137**: 274-286.

856 **Pattathil, S., Harper, A. D., & Bar-Peled, M. (2005).** Biosynthesis of UDP-xylose:
857 characterization of membrane-bound AtUXS2. *Planta*, **221**: 538-548.

858 **Peaucelle, A., Louvet, R., Johansen, J. N., Höfte, H., Laufs, P., Pelloux, J., and Mouille,**
859 **G. (2008).** Arabidopsis phyllotaxis is controlled by the methyl-esterification status of cell-wall
860 pectins. *Current Biology*, **18**: 1943-1948.

861 **Ralet, M.C., Crépeau, M.J., Vigouroux, J., Tran, J., Berger, A., Sallé, C., Granier, F.,**
862 **Botran, L. and North, H.M. (2016).** Xylans provide the structural driving force for mucilage
863 adhesion to the Arabidopsis seed coat. *Plant Physiol.*, **171**: 165-178.

864 **Rautengarten, C., Ebert, B., Herter, T., Petzold, C.J., Ishii, T., Mukhopadhyay, A.,**
865 **Usadel, B., and Scheller, H.V. (2011).** The interconversion of UDP-arabinopyranose and
866 UDP-arabinofuranose is indispensable for plant development in Arabidopsis. *Plant Cell* **23**:
867 1373–1390.

868 **Rautengarten, C., Ebert, B., Moreno, I., Temple, H., Herter, T., Link, B., Doñas-Cofré,**
869 **D., Moreno, A., Saéz-Aguayo, S., Blanco, F., Mortimer, J.C., Schultink, A., Reiter, W.-D.,**
870 **Dupree, P., Pauly, M., Heazlewood, J., Scheller, H. and Orellana, A. (2014).** The Golgi
871 localized bifunctional UDP-rhamnose/UDP-galactose transporter family of Arabidopsis. *Proc.*
872 *Natl. Acad. Sci.* **111**: 11563–11568.

873 **Rautengarten, C., Ebert, B., Liu, L., Stonebloom, S., Smith-Moritz, A. M., Pauly, M., et**
874 **al. (2016).** The Arabidopsis Golgi-localized GDP-L-fucose transporter is required for plant
875 development. *Nature Communications*, **7**.

876 **Reboul, R., Geserick, C., Pabst, M., Frey, B., Wittmann, D., Lütz-Meindl, U., Léonard,**
877 **R., and Tenhaken, R. (2011).** Down-regulation of UDP-glucuronic acid biosynthesis leads to
878 swollen plant cell walls and severe developmental defects associated with changes in pectic
879 polysaccharides. *J. Biol. Chem.* **286**: 39982–39992.

880 **Reyes, F., and Orellana, A. (2008).** Golgi transporters: opening the gate to cell wall
881 polysaccharide biosynthesis. *Curr. Opin. Plant Biol.* **11**: 244–251.

882 **Reyes, F., Marchant, L., Norambuena, L., Nilo, R., Silva, H., and Orellana, A. (2006).**
883 AtUTr1, a UDP-glucose/UDP-galactose transporter from Arabidopsis thaliana, is located in
884 the endoplasmic reticulum and up-regulated by the unfolded protein response. *J. Biol.*
885 *Chem.* **281**: 9145–9151.

886 **Reyes, F., León, G., Donoso, M., Brandizzi, F., Weber, A.P.M., and Orellana, A. (2010).**
887 The nucleotide sugar transporters AtUTr1 and AtUTr3 are required for the incorporation of
888 UDP-glucose into the endoplasmic reticulum, are essential for pollen development and are
889 needed for embryo sac progress in Arabidopsis thaliana. *Plant J.* **61**: 423–435.

890 **Rollwitz, I., Santaella, M., Hille, D., Flügge, U.-I., and Fischer, K. (2006).** Characterization
891 of AtNST-KT1, a novel UDP-galactose transporter from Arabidopsis thaliana. *FEBS Lett.*
892 **580**: 4246–4251.

893 **Rösti, J., Barton, C.J., Albrecht, S., Dupree, P., Pauly, M., Findlay, K., Roberts, K. and**
894 **Seifert, G.J. (2007).** UDP-glucose 4-epimerase isoforms UGE2 and UGE4 cooperate in

895 providing UDP-galactose for cell wall biosynthesis and growth of *Arabidopsis thaliana*. *Plant*
896 *Cell*, **19**: 1565-1579.

897 **Saez-Aguayo, S., Ralet, M.-C., Berger, A., Botran, L., Ropartz, D., Marion-Poll, A., and**
898 **North, H.M.** (2013). PECTIN METHYLESTERASE INHIBITOR6 promotes *Arabidopsis*
899 mucilage release by limiting methylesterification of homogalacturonan in seed coat
900 epidermal cells. *Plant Cell* **25**: 308–323.

901 **Saint-Jore-Dupas, C., Nebenführ, A., Boulaflous, A., Follet-Gueye, M.-L., Plasson, C.,**
902 **Hawes, C., Driouich, A., Faye, L., and Gomord, V.** (2006). Plant N-glycan processing
903 enzymes employ different targeting mechanisms for their spatial arrangement along the
904 secretory pathway. *Plant Cell* **18**: 3182–3200.

905 **Scheible, W.-R., and Pauly, M.** (2004). Glycosyltransferases and cell wall biosynthesis:
906 novel players and insights. *Curr. Opin. Plant Biol.* **7**: 285–295.

907 **Seifert, G. J.** (2004). Nucleotide sugar interconversions and cell wall biosynthesis: how to
908 bring the inside to the outside. *Curr. Opin. Plant Biol.*, **7**: 277-284.

909 **Sterling, J.D., Quigley, H.F., Orellana, A., and Mohnen, D.** (2001). The catalytic site of the
910 pectin biosynthetic enzyme alpha-1,4-galacturonosyltransferase is located in the lumen of
911 the Golgi. *Plant Physiol.* **127**: 360–371.

912 **Truernit, E., Bauby, H., Dubreucq, B., Grandjean, O., Runions, J., Barthélémy, J., and**
913 **Palauqui, J.-C.** (2008). High-resolution whole-mount imaging of three-dimensional tissue
914 organization and gene expression enables the study of Phloem development and structure
915 in *Arabidopsis*. *Plant Cell* **20**: 1494–1503.

916 **Temple, H., Saez-Aguayo, S., Reyes, F. C., and Orellana, A.** (2016). The inside and
917 outside: topological issues in plant cell wall biosynthesis and the roles of nucleotide sugar
918 transporters. *Glycobiology* **26**: 913-925.

919 **Tusnády, G.E. and Simon, I.** (2001) The HMMTOP transmembrane topology prediction
920 server. *Bioinformatics* **17**: 849-850

921 **Verhertbruggen, Y., Marcus, S.E., Haeger, A., Ordaz-Ortiz, J.J., and Knox, J.P.** (2009).
922 An extended set of monoclonal antibodies to pectic homogalacturonan. *Carbohydr. Res.*
923 **344**: 1858–1862.

924 **Voiniciuc, C., Günl, M., Schmidt, M.H.-W., and Usadel, B.** (2015). Highly Branched Xylan
925 Made by IRREGULAR XYLEM14 and MUCILAGE-RELATED21 Links Mucilage to
926 *Arabidopsis* Seeds. *Plant Physiol.* **169**: 2481–2495.

927 **Western, T.L.** (2012). The sticky tale of seed coat mucilages: production, genetics, and role
928 in seed germination and dispersal. *Seed Sci. Res.* **22**: 1–25.

929 **Western, T.L., Burn, J., Tan, W.L., Skinner, D.J., Martin-McCaffrey, L., Moffatt, B.A.,**
930 **and Haughn, G.W.** (2001). Isolation and Characterization of Mutants Defective in Seed Coat
931 Mucilage Secretory Cell Development in *Arabidopsis*. *Plant Physiol.* **127**: 998–1011.

932 **Western, T. L., Skinner, D. J., & Haughn, G. W.** (2000). Differentiation of mucilage
933 secretory cells of the *Arabidopsis* seed coat. *Plant Physiol.*, **122**: 345-356.

934 **Western, T.L., Young, D.S., Dean, G.H., Tan, W.L., Samuels, A.L., and Haughn, G.W.**
935 (2004). MUCILAGE-MODIFIED4 Encodes a Putative Pectin Biosynthetic Enzyme
936 Developmentally Regulated by APETALA2, TRANSPARENT TESTA GLABRA1, and
937 GLABRA2 in the *Arabidopsis* Seed Coat. *Plant Physiol.* **134**: 296–306.

938 **Willats, W.G., McCartney, L., and Knox, J.P.** (2001). In-situ analysis of pectic
939 polysaccharides in seed mucilage and at the root surface of *Arabidopsis thaliana*. *Planta*
940 **213**: 37–44.

- 941 **Winter, D., Vinegar, B., Nahal, H., Ammar, R., Wilson, G.V., Provart, N.J.** (2007) An
942 “electronic fluorescent pictograph” browser for exploring and analyzing large-scale biological
943 data sets. *PLoS ONE* **2**: e718.
- 944 **Wulff, C., Norambuena, L., and Orellana, A.** (2000). GDP-fucose uptake into the Golgi
945 apparatus during xyloglucan biosynthesis requires the activity of a transporter-like protein
946 other than the UDP-glucose transporter. *Plant Physiol.* **122**: 867–877.
- 947 **Yang, T., Bar-Peled, L., Gebhart, L., Lee, S.G., and Bar-Peled, M.** (2009). Identification of
948 Galacturonic Acid-1-phosphate Kinase, a New Member of the GHMP Kinase Superfamily in
949 Plants, and Comparison with Galactose-1-phosphate Kinase. *J. Biol. Chem.* **284**: 21526–
950 21535.
- 951 **Young, R.E., McFarlane, H.E., Hahn, M.G., Western, T.L., Haughn, G.W., and Samuels,**
952 **A.L.** (2008). Analysis of the Golgi apparatus in *Arabidopsis* seed coat cells during polarized
953 secretion of pectin-rich mucilage. *Plant Cell* **20**: 1623–1638.
- 954 **Zablackis, E., Huang, J., Muller, B., Darvill, A.G., and Albersheim, P.** (1995).
955 Characterization of the Cell-Wall Polysaccharides of *Arabidopsis thaliana* Leaves. *Plant*
956 *Physiol.* **107**:1129–1138.
- 957
- 958

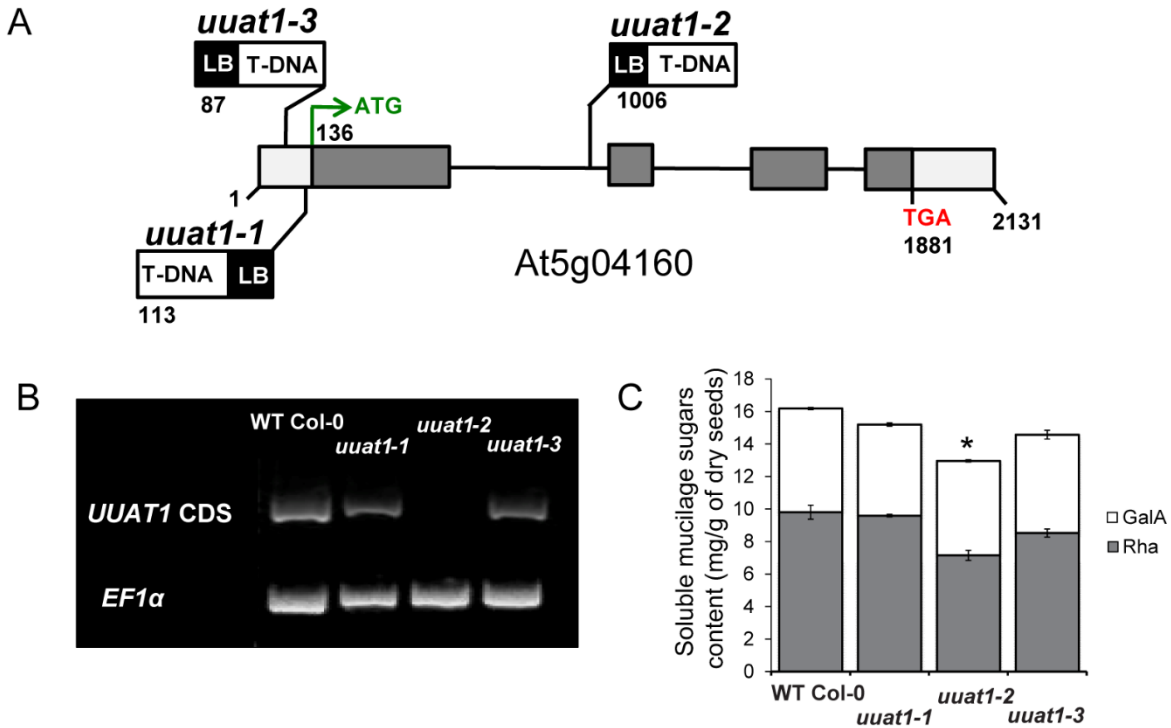


Figure 1. Characterization of Mutants in *UAT1*.

(A) Schematic representation of *UAT1* structure, as annotated in The Arabidopsis Information Resource (TAIR: <http://www.arabidopsis.org/>). The sites and orientations of the T-DNA insertions in allelic lines *uuat1-1*, *uuat1-2* and *uuat1-3* are indicated. Numbers indicate the positions (in bp) of the start and stop codons and the T-DNA insertion sites. White boxes, 5'- and 3'-UTRs; grey boxes, protein coding sequences; black lines, introns; LB, left border.

(B) Analysis of *UAT1* expression in T-DNA insertion lines. RT-PCR analyses were performed on RNAs isolated from WT Col-0, *uuat1-1*, *uuat1-2* and *uuat1-3* lines using specific primers for the full-length coding sequence of *UAT1*. *EF1α* expression was used as a control.

(C) Measurement of galacturonic acid and rhamnose levels in soluble mucilage after 10 min of seed imbibition in water. Error bars represent SE ($n = 6$) of 3 biological replicates. * Significant difference from WT using the t-test $p < 0.05$.

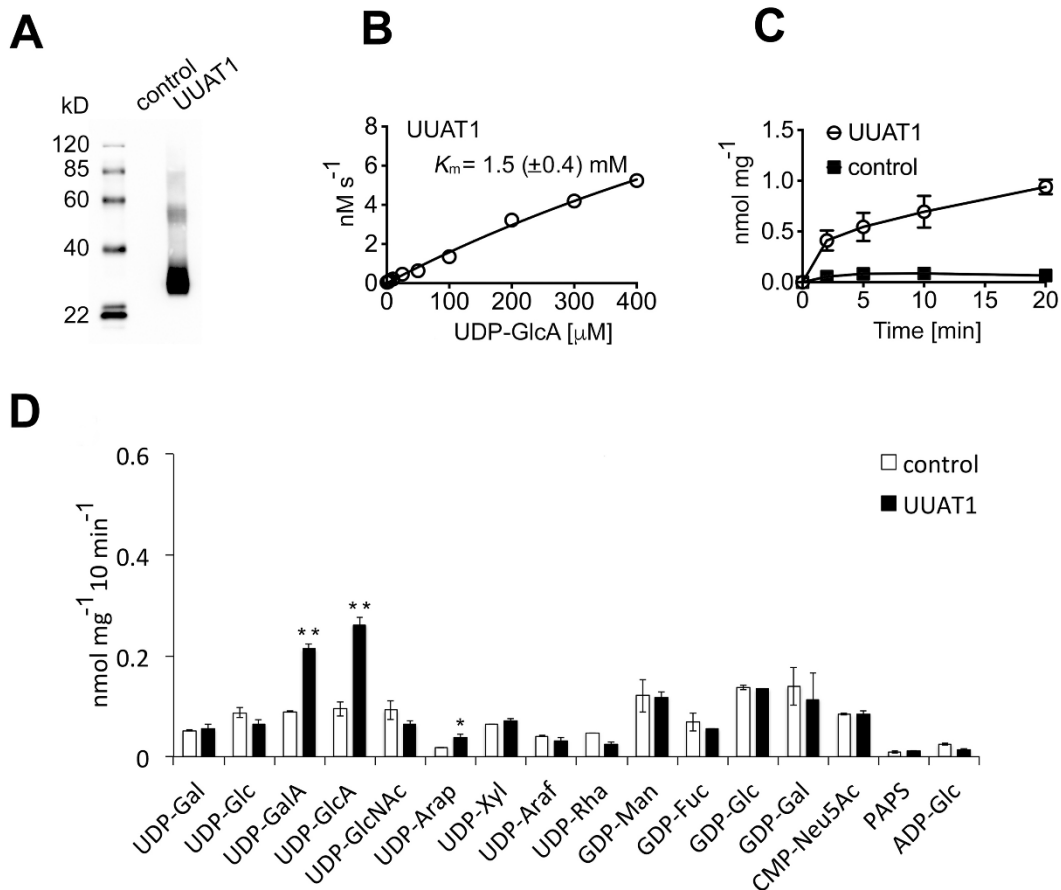


Figure 2. UUAT1 is a UDP-Uronic Acid Transporter.

(A) Immunoblot of the yeast microsomal fractions used to make the proteoliposomes. 2.5 μg total protein was probed with an anti-V5 tag antibody and strong expression of UUAT1 (~35 kDa) was observed.

(B) Kinetics of UDP-GlcA transport at varying concentrations (0.5 to 400 μM) into proteoliposomes pre-loaded with UMP and then incubated for 2 min at 25°C.

(C) Time course for UDP-GlcA (50 μM) uptake into proteoliposomes preloaded with UMP and then incubated at 25°C. All values were normalized to the total protein content of the proteoliposome preparations and are means \pm SD of 4 independent experiments.

(D) Quantification of nucleotide sugar uptake into proteoliposomes containing UUAT1 that were preloaded with UMP. Data are the means \pm SD of four independent transport assays quantified by LC-MS/MS and normalized to the total protein content of the reconstituted proteoliposomes. The empty expression vector was used as a negative control. Significantly different values are marked with asterisks: * $p < 0.05$ and ** $p < 0.01$; Student's t -test.

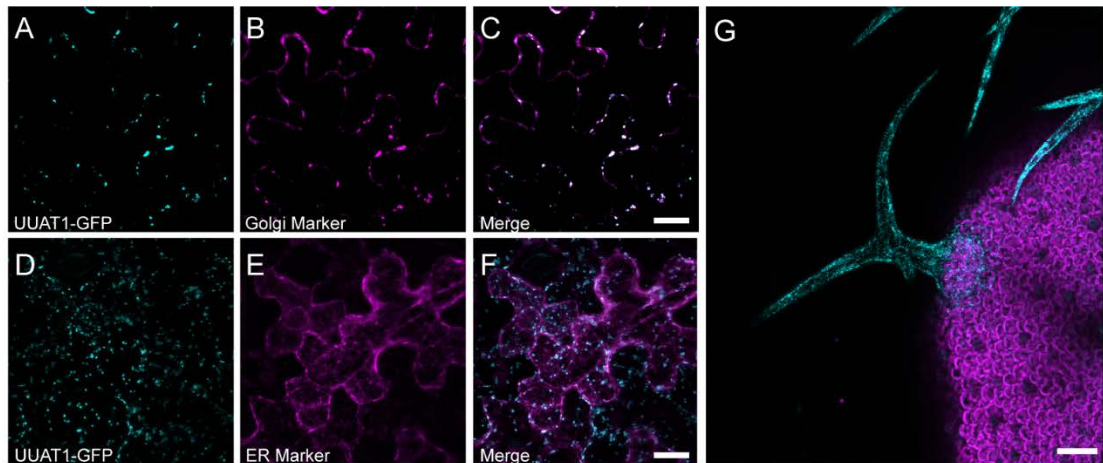


Figure 3. UUAT1 is Located in the Golgi Apparatus.

(A) to (F) Tobacco epidermal cells were co-transformed with Agrobacteria carrying vectors containing *Pro35S:UUAT1-GFP* with the *cis*-Golgi marker α -Mannosidase-I-Cherry (A) to (C) or the endoplasmic reticulum marker wall-associated kinase-2-signal peptide-mCherry-HDEL (D) to (F). GFP labelling co-localized with the Golgi marker (C) but not with the ER marker (F). Bar = 5 μ m.

(G) Subcellular localization of UUAT1-GFP in trichomes from *uuat1-2* plants rescued with the *ProUUAT1:UUAT1-GFP* construct; Bar = 100 μ m.

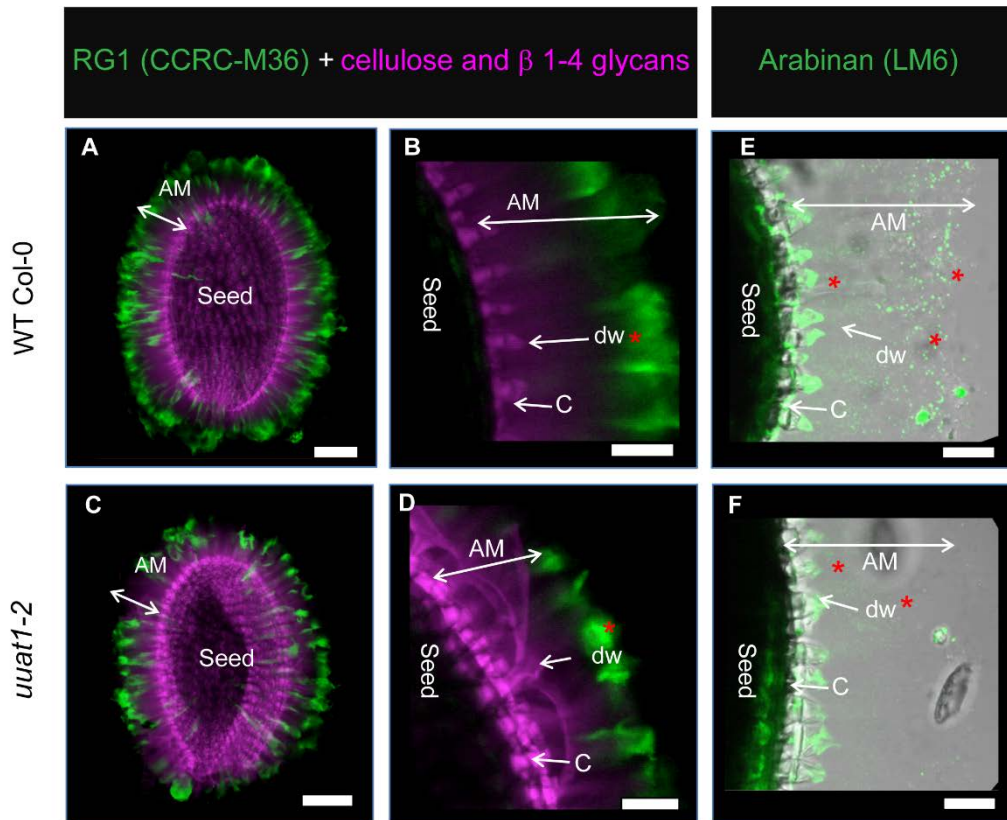


Figure 4. The *uuat1-2* Mutant is Affected in Seed Mucilage Structure and Composition

(A) to (F) RG-I and arabinan labelling in adherent mucilage from WT Col-0 seeds and the *uuat1-2* mutant line. Confocal microscopy optical section reconstruction of adherent mucilage (AM) released from imbibed seeds. Asterisks represent differences in labeling.

(A) to (D) CCRC-M36 antibody (green) was used to label RG-I domains and calcofluor white was used to detect β -1,4-glucans (purple). (B) and (D) are magnifications of parts (A) and (C) showing greater detail of the AM, the distal cell wall (dw) and the columella cells (c).

(E) and (F) The LM6 antibody was used to label arabinan (green) in both WT Col-0 and *uuat1-2* seeds. Bars = (A) and (C), 100 μ m; (B) to (F), 50 μ m.

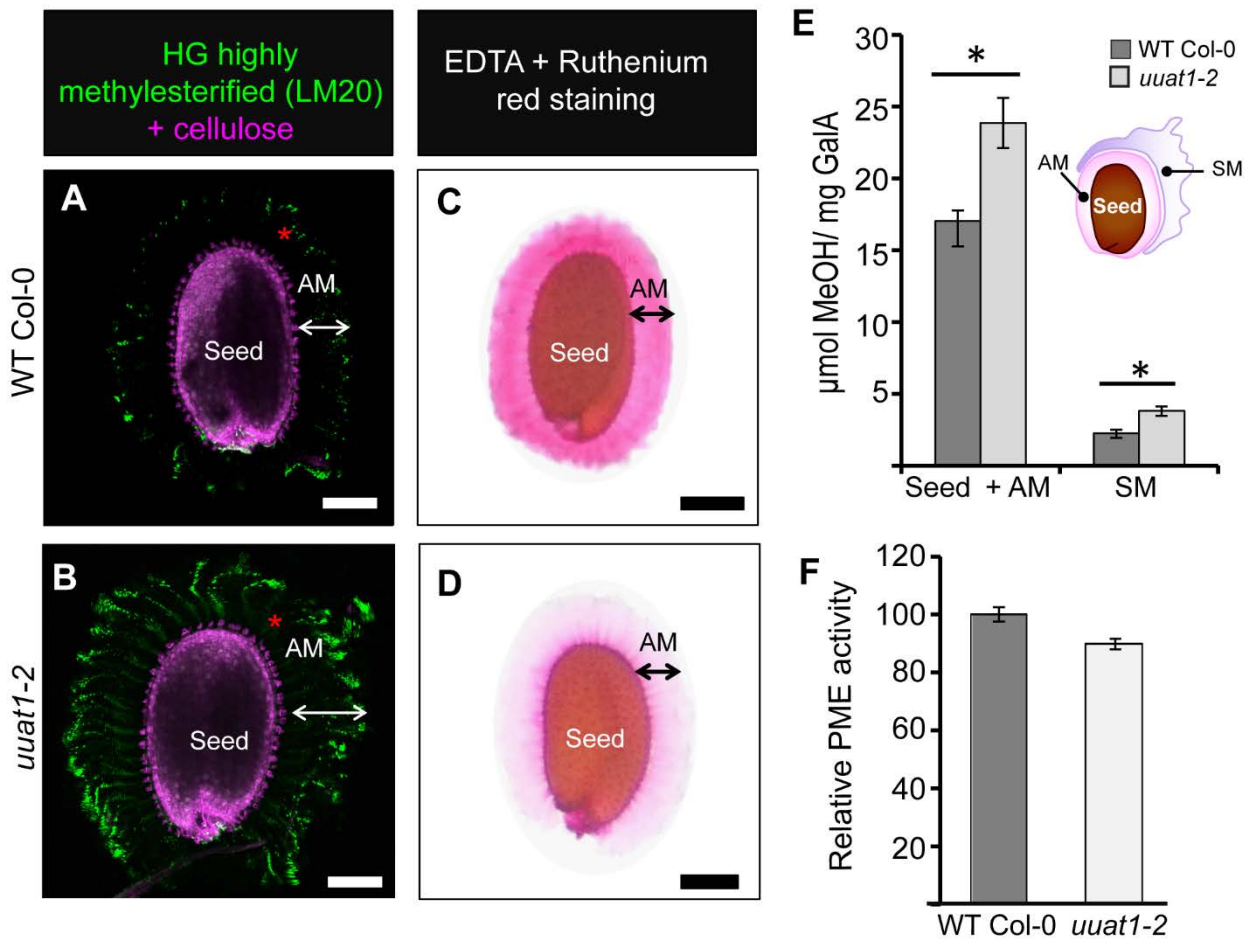


Figure 5. The *uuat1-2* Mutant Shows Increased Pectin Methylesterification and Has Reduced Pectin Methylesterase Activity in Seeds.

(A) and (B) Labeling of highly methylesterified HG in the adherent mucilage from seeds of WT Col-0 **(A)** and the *uuat1-2* mutant line **(B)**. Confocal microscopy optical section reconstruction of AM released from imbibed seeds. The LM20 antibody (green) was used to label HG domains and propidium iodide was used to stain the seed coat surface (pink). Bars = 100 μm ; AM, adherent mucilage.

(C) and (D) Appearance of seed adherent mucilage from WT Col-0 **(C)** and *uuat1-2* **(D)** in the presence of a cation chelator. Seeds were stained with ruthenium red after 1 h of imbibition in 0.5 M EDTA. AM, adherent mucilage. Bars = 100 μm .

(E) Degree of methylesterification in WT Col-0 and *uuat1-2* in seed + AM and the soluble mucilage fractions. Error bars represent SE (n = 16, from 3 biological replicates). ANOVA and Tukey tests were performed and compared to WT Col-0 (*p < 0.05).

(F) Seed pectin methylesterase (PME) activity. Total protein extracts from mature dry seeds of WT Col-0 and *uuat1-2* were used to measure PME activity. The PME activity was normalized to the average wild-type activity (100). Error bars represent SE (n = 16 for SM and n = 12 for seed + AM from 3 biological replicates).

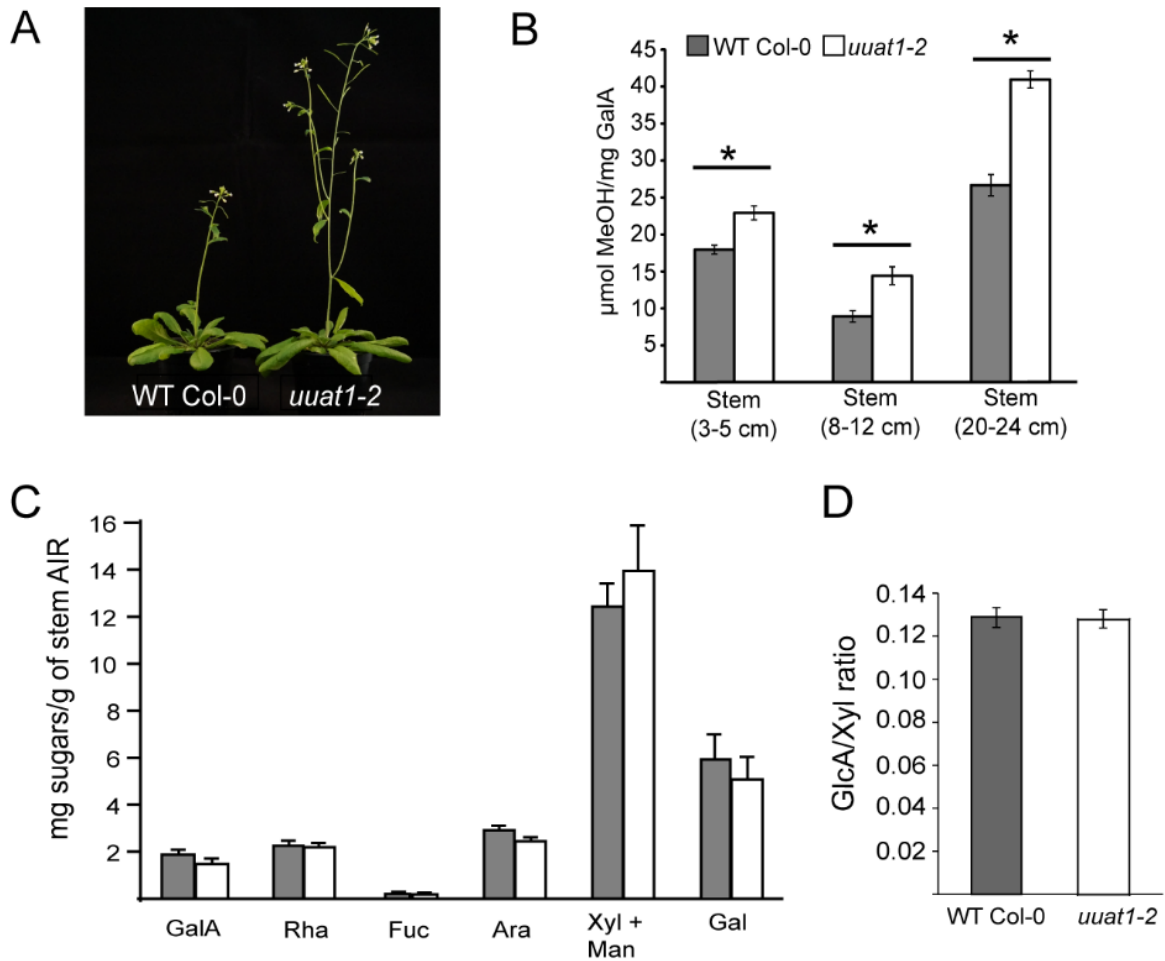


Figure 6. The *uuat1-2* Mutant Line Displays an Early Stem Elongation Phenotype and an Increase in Methylesterification, but Shows No Changes in Sugar Content in Stem Cell Walls.

(A) The *uuat1-2* mutant displays early stem elongation when compared to the WT Col-0. 7 week-old WT Col-0 and *uuat1-2* plants show a pronounced difference in stem height. This difference disappears once the plants reach their adult state. This phenotype was observed in 3 biological replicates.

(B) Determination of the degree of methylesterification in stems. Error bars represent SE (n = 8) from 2 biological replicates. Asterisks represent significant difference from WT Col-0 using ANOVA and Tukey tests (p < 0.05).

(C) HPAEC-PAD was used to quantify the cell wall extract monosaccharide composition from WT Col-0 and *uuat1-2* stems (20-24 cm). Error bars represent SE (n = 6) from 3 biological replicates.

(D) Ratio of GlcA/Xyl content of xylan products digested with GH11 xylanase. AIR material from basal stems of WT Col-0 and *uuat1-2* was used to determine the frequency of GlcA branches on the xylan backbone using PACE. The quantity of each of the oligosaccharides released by GH11 xylanase [Xyl, (Xyl)₂, GlcA-(Xyl)₄/MeGlcA(Xyl)₄] was calculated and the GlcA/Xyl ratio determined. Error bars represent SE (n = 9) from 3 biological replicates.

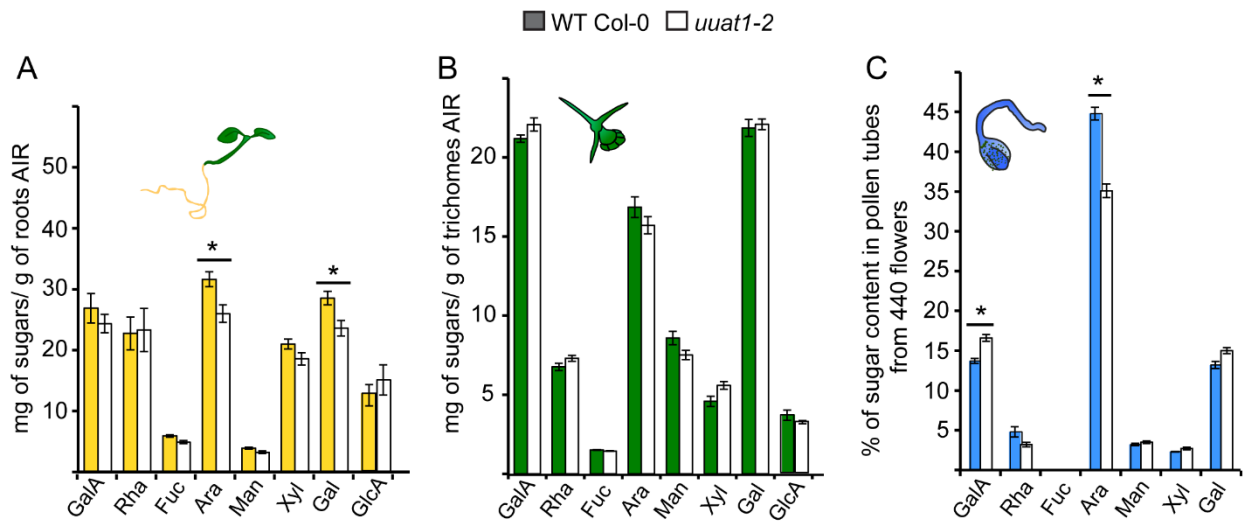


Figure 7. Monosaccharide Composition of Different Organs, Tissues or Cells from WT Col-0 and *uuat1-2* Mutant Plants.

(A) to (C) Quantification of the monosaccharide composition of the cell wall extracts from WT Col-0 and *uuat1-2* mutant plants using HPAEC-PAD and GC-FID.

(A) Roots from 7 d-old plants.

(B) Trichomes from 14 d-old plants.

(C) Pollen tubes from 6 h-old plants. Error bars represent SE (n = 6) from 3 biological replicates. * Significant differences from WT using the Wilcoxon test ($p < 0.05$).